2 Single-Phase Flow Equations and Regimes

The primary assumptions and formulations for single-phase flow regimes are reviewed in this chapter. The governing partial differential equations for general fluid dynamics are developed in §2.1, while equations of state and associated flow regimes are developed in §2.2. Assuming incompressible conditions, flow rotation and the stream function are discussed in §2.3, while inviscid hydrodynamics are presented in §2.4. Viscous effects are reintroduced in §2.5 along with the Reynolds number. The various viscous regimes are characterized via the Reynolds number in §2.6 and flow instability mechanisms are introduced in §2.7. For additional discussion of single-phase fluid dynamics equations, the reader is referred to White (2016) and Schlichting and Gertsen (2017).

It should be noted that the fluid dynamic discussion and governing equations in this chapter assume a continuum flow (§1.5) whereby the flow properties vary smoothly in space and time. For a body in such a continuum surrounding gas, the length scale of any fluid gradients must be much larger than the mean free path of the molecules, that is, the Knudsen number based on a differential length scale must be very small.

In terms of notation, the single-phase fluid velocity and pressure in this chapter will be defined using $\mathbf{u}$ and p, but the equations apply equally with $\mathbf{U}$ and P_f as the variables for single-phase flow. As such, the Chapter 2 single-phase equations can be extended to multiphase flow for either the unhindered or resolved-surface flow fields as discussed in §1.4. These equations can also be used to describe the flow inside a particle using $\mathbf{V}$ and P_p as the variables.

2.1 Conservation Equations and Fluid Properties

The transport partial differential equations (PDEs) that govern single-phase flows are based on the conservation of mass, momentum, energy, and species. These equations can be developed using the Reynolds transport theorem (RTT) and the associated fluid properties. In the following, this transport theorem is defined and then employed to develop transport PDEs for fluid density, velocity, temperature, and species concentration. For use in these transport equations, we will define fluid properties such as bulk and kinematic viscosity, total and internal fluid energy, as well as thermal and molecular diffusivity. In addition, this chapter will present several dimensionless parameters to characterize flow regimes, including the Froude, Mach, Prandtl, Reynolds, and Schmidt numbers.

https://doi.org/10.1017/9781139028806.003 Published online by Cambridge University Press

2.1.1 Reynolds Transport Theorem and Mass Conservation

Reynolds Transport Theorem of a Fluid

The Reynolds transport theorem states that the time rate of change of a transport quantity within a control volume is equal to the sum of the net inward flux through the control volume's surface and the internal generation rate of the same quantity within the volume. In more concise terms, the rate of increase of a quantity in a volume equals the flux rate across the boundary plus the generation rate within the volume.

The RTT concept can determine the time rate of change of a moving quantity for a wide range of scenarios. For example, the rate change of a specific animal population in a game reserve is the sum of the flux through the region's boundary (which will be positive if more animals cross into the region) and the rate of internal generation (which will be positive if the birth rate exceeds the death rate). The RTT concept can be applied to other transported quantities, such as goods, money, diseases, and so on. In some cases, a quantity can move by convection, and in other cases it can be spread by diffusion. For example, a chemical in a still pond can diffuse by molecular motion (spread out) within the pond or it can convect downstream (move with fluid velocity) and be released in a river. In other cases, only convection is important. For example, the mass of water in a still pond does not diffuse (assuming the containing surface is not porous), but it can convect downstream in a river.

The RTT can also be applied in fluid dynamics to determine the relevant equations of motion. To do this, we must first differentiate between an "intensive" quantity and an "extensive" fluid quantity. An extensive property is proportional to the volume considered for uniform conditions. For example, the mass of a fluid is extensive as it will increase as the measuring volume increases. In contrast, an intensive quantity is one that is independent of the measuring volume size for uniform conditions. For example, density (mass of fluid per unit volume) is intensive since it will be the same throughout a uniform flow, regardless of the size of measuring volume employed.

To convert the RTT text into a PDE, consider an intensive quantity (q) that moves locally at a velocity $(\mathbf{u})$ throughout a fixed control volume $(\forall)$ with a defined control surface area (A) and outward normal unit vector $(\mathbf{n})$, as shown in Figure 2.1. The RTT volume-based terms can be expressed as volume integrals of the intensive quantity (q), while the flux-based terms can be expressed as surface integrals based on convection $(\mathbf{u})$ and diffusion rate $(\mathbf{Q})$, as follows:

$$\frac{\partial}{\partial \mathrm{t}} \iiint_{\forall} \mathrm{q}\, \mathrm{d}\forall = -\oiint_{\mathrm{A}} \mathrm{q}(\mathbf{u}\cdot\mathbf{n})\, \mathrm{dA} - \oiint_{\mathrm{A}} \mathbf{Q}\cdot\mathbf{n}\, \mathrm{dA} + \iiint_{\forall} \dot{\mathrm{q}}\, \mathrm{d}\forall. \tag{2.1}$$

Each term in this equation is discussed in the following paragraph.

The left-hand side (LHS) of (2.1) is the time rate of change of q integrated over the control volume based on the Eulerian time derivative (i.e., based on a fixed point in space). As a result of the volume integral, the integrated time rate of change represented by the LHS is an extensive quantity. For example, if q is density, the LHS represents the time rate of change of the control volume mass. The first term on the right-hand side (RHS) is the flux across the boundary due to convection. This term can

https://doi.org/10.1017/9781139028806.003 Published online by Cambridge University Press

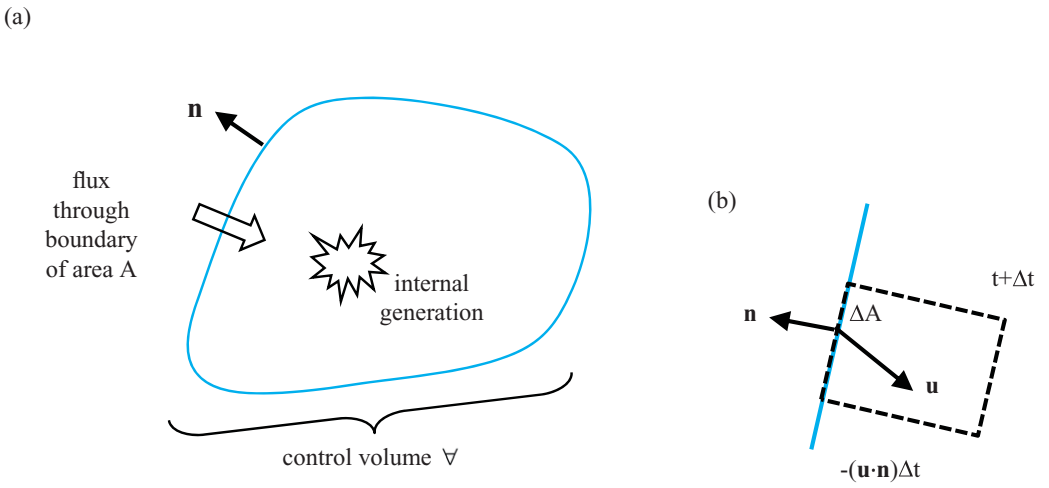

Figure 2.1 (a) Reynolds transport theorem schematic for an arbitrary control volume ($\forall$) where total change in time of a transported intensive quantity is equal to the sum of its (convective and nonconvective) flux through the boundary (which has surface area A and outward normal vector **n**) and of its internal generation, and (b) representation of the convective flux through a local surface element area (ΔA) where the fluid moves at velocity **u** such that the amount of fluid that fluxes into the domain over a time Δt is given by $-(\mathbf{u} \cdot \mathbf{n})(\Delta t)(\Delta A)$.

be obtained by considering a fluid element crossing a differential surface area (ΔA), as shown in Figure 2.1b. Note that only the movement perpendicular to the surface contributes to the flux since tangential movement makes no contribution. Over a time Δt, the fluid element moving perpendicularly into this surface has a length displacement given by $-\mathbf{u} \cdot \mathbf{n}\, \Delta t$, where the negative sign is required to describe inward flux. Taking Δt and ΔA to be infinitesimally small, the flux rate (the first term on the RHS of (2.1) becomes the surface integral of the product of the quantity per unit volume (q) and the penetration volume per unit time $(-\mathbf{u} \cdot \mathbf{n}\, dA)$. The second term on the RHS includes the diffusive flux rate $(\mathbf{Q})$, which is the rate of flux of q through the surface that spreads due to nonconvective effects. This nonconvective flux rate is zero for mass and momentum conservation, but it is nonzero for energy transport (due to thermal conduction) and species transport (due to species diffusion). The third and final term on the RHS of (2.1) is the volume integral of the internal generation rate $(\dot{q})$, which is the net rate at which a quantity is created (or destroyed if a negative value) within the control volume.

The integral-based RTT form shown in (2.1) for fluid dynamics can be transformed into a PDE, which is often more practical to employ, by first converting the surface integrals into volume integrals. For this, we assume that q and **u** are finite and continuously differentiable in space and that the control volume is time invariant (e.g., the volume has fixed shape and a single fixed speed or is stationary). Based on these assumptions, one can employ the Gauss divergence theorem so that the surface integral of the flux terms (using the surface outward normal **n**) can be transformed into a volume integral, as follows:

https://doi.org/10.1017/9781139028806.003 Published online by Cambridge University Press

$$\oiint_{A} [q(\mathbf{u}\cdot\mathbf{n}) + \mathbf{Q}\cdot\mathbf{n}]\, dA = \iiint_{\forall} [\nabla\cdot(q\mathbf{u}) + \nabla\cdot\mathbf{Q}]\, d\forall. \tag{2.2}$$

By combining (2.1) and (2.2), all the terms can be consistently expressed as volume integrals. Since the size and location of the volume integral is arbitrary, an infinitesimally small volume with locally uniform flow allows the integrands to be equated, yielding the following:

$$\frac{\partial q}{\partial t} + \nabla\cdot(q\mathbf{u} + \mathbf{Q}) = \dot{q}. \tag{2.3}$$

This is the Eulerian Reynolds transport PDE for an intensive fluid quantity.

The Lagrangian version of this equation can be obtained by employing (1.17b) for the time derivative of q and rewriting the dot product term using the following gradient product vector identity:

$$\frac{\mathcal{D}q}{\mathcal{D}t} \equiv \frac{\partial q}{\partial t} + \mathbf{u}\cdot\nabla q = \frac{\partial q}{\partial t} + \nabla\cdot(q\mathbf{u}) - q(\nabla\cdot\mathbf{u}). \tag{2.4}$$

Combining this result with (2.3) yields the Lagrangian Reynolds transport PDE (along the fluid path):

$$\frac{\mathcal{D}q}{\mathcal{D}t} + q(\nabla\cdot\mathbf{u}) + \nabla\cdot\mathbf{Q} = \dot{q}. \tag{2.5}$$

These results for the Reynolds transport of an intensive fluid quantity can be used to obtain the transport equations for fluid mass, momentum, total energy, and species per unit volume. In cases where diffusion can be neglected (as will be shown for transport of fluid mass or momentum), $\mathbf{Q} = 0$, so this equation is simplified accordingly.

Transport of Mass

For the mass transport equation, the transport PDE is obtained by setting q to be the fluid density (ρ_f). If we assume that mass is neither created nor destroyed (no nuclear reactions), then $\dot{\rho}_f = 0$ for a single-phase flow. Furthermore, we can assume that mass only moves by convection so that the diffusive fluxes can be neglected ($\mathbf{Q} = 0$). As such, application of (2.3) and (2.5) yields the following Eulerian and Lagrangian mass transport PDEs for fluid mass:

$$\frac{\partial \rho_f}{\partial t} + \nabla\cdot(\rho_f\mathbf{u}) = 0. \tag{2.6a}$$

$$\frac{\mathcal{D}\rho_f}{\mathcal{D}t} + \rho_f(\nabla\cdot\mathbf{u}) = 0. \tag{2.6b}$$

These PDEs are referred to as the conservation of mass or the continuity equations. The Eulerian PDE (2.6a) shows that the rate of density change at a point is related to the divergence of momentum per unit volume, while the Lagrangian PDE (2.6b) shows that the rate of density change along a fluid streamline is related to the divergence of the fluid velocity.

https://doi.org/10.1017/9781139028806.003 Published online by Cambridge University Press

The Eulerian transport PDE (2.6a) can be expressed in Cartesian component form or in tensor form as shown in the following:

$$\frac{\partial \rho_f}{\partial t} + \frac{\partial}{\partial x}(\rho_f u_x) + \frac{\partial}{\partial y}(\rho_f u_y) + \frac{\partial}{\partial z}(\rho_f u_z) = 0, \tag{2.7a}$$

$$\frac{\partial \rho_f}{\partial t} + \frac{\partial}{\partial X_i}(\rho_f u_i) = 0 \qquad \textit{for } i = 1, 2, \textit{and } 3. \tag{2.7b}$$

The Lagrangian version can be similarly expanded in Cartesian component or tensor form. Furthermore, spherical versions of the Eulerian and Lagrangian mass transport PDEs can be obtained using the divergence defined in (1.11a).

If the volume of the fluid element can change in shape but does not change in size because it is incompressible and the quantity does not diffuse, it has constant mass and thus constant density along the fluid path This is defined as an *isochoric* flow and its Lagrangian time derivative is zero. Based on (2.6b), this indicates that the divergence of the velocity field must then also be zero:

$$\nabla \cdot \mathbf{u} = \mathbf{0} \qquad \textit{for constant density along fluid path.} \tag{2.8}$$

As such, the "divergence-free" flow of (2.8) is equivalent to stating that the fluid density is constant (and incompressible) along its fluid path. This is a convenient mathematical simplification that will be used later for appropriate flow conditions.

2.1.2 Transport of Momentum

The momentum transport equation can be obtained by setting the intensive transport quantity as the fluid momentum per unit volume ($\mathbf{q} = \rho_f \mathbf{u}$) and applying RTT using (2.1)–(2.5). In doing so, we note that fluid momentum cannot diffuse (it can only be transported by velocity), so $\mathbf{Q} = 0$ for each of the three momentum components. Next, we consider the last term in (2.1), which describes internal generation rate, for fluid momentum. Since momentum can be changed (accelerated or decelerated) via Newton's second law ($\mathbf{F} = m\mathbf{a}$), the rate of this change per unit volume at a fixed location is equal to the sum of the applied forces per unit volume:

$$\dot{\mathbf{q}}_{mom} = \mathbf{F}_{fluid}/\forall_f = \left(\mathbf{F}_{body} + \mathbf{F}_{surf}\right)/\forall_f. \tag{2.9}$$

The RHS shows that the forces acting on a fluid element include body forces (proportional to mass) and surface forces (proportional to surface area), where both are discussed in the following.

Body forces are those forces which are proportional to the mass of an object and can generally include gravitational, electrostatic, and magnetic body forces. Since electrostatic and magnetic forces are generally weak in two-phase flows, they will be neglected in this textbook so gravitational force is the only body force. This force is based on the mass of fluid and gravity (where $\mathbf{g}$ is the gravity acceleration vector), as follows:

$$\mathbf{F}_{body} = m_f \mathbf{g} = \rho_f \forall_f \mathbf{g} \tag{2.10}$$

https://doi.org/10.1017/9781139028806.003 Published online by Cambridge University Press

As shown by the RHS using fluid density, the gravity force per unit volume is $\rho_f \mathbf{g}$.

The surface forces in fluid dynamics are the pressure forces and the viscous forces, where both are a product of stress and an area. The pressure acts perpendicular to a surface area with a stress given by the pressure (p). The viscous stresses can act both perpendicularly and tangentially to a surface and are related to the flow viscosity and the gradients in flow velocity. In the following, we obtain their combined effect in mathematical form.

The pressure and viscous stresses can be obtained by considering an elemental volume $(\Delta x \Delta y \Delta z)$, as shown in Figure 2.2. For example, we can consider the effects of the pressure force in the y-direction and assume there is a pressure difference (Δp) due to a gradient, as shown in Figure 2.2a. Since pressure only acts normal to a surface, the y-direction force is based only on the top and bottom surfaces, whose area is $\Delta x \Delta z$. Since the pressure acts on the volume toward the surface (inward normal),

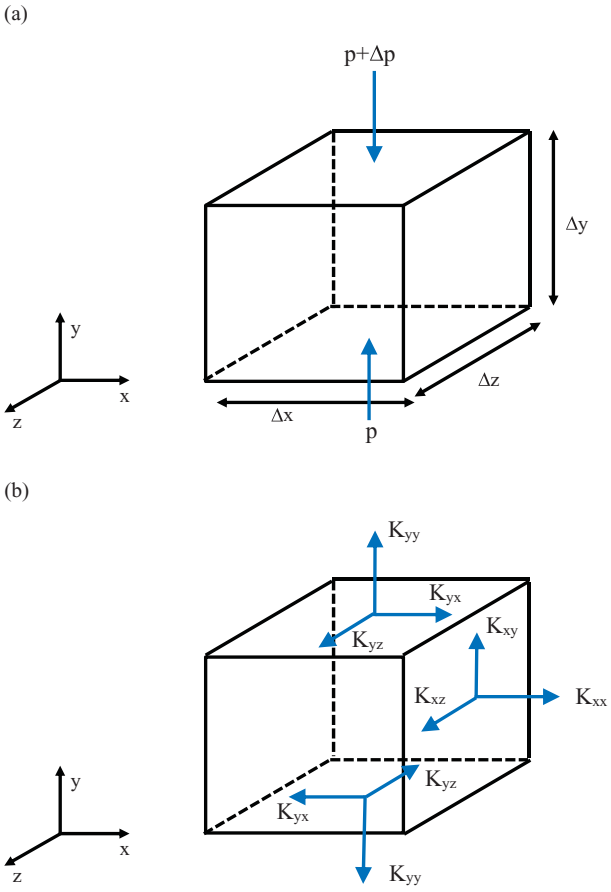

Figure 2.2 Fluid dynamic stresses on a fluid element with a discrete volume $(\Delta x \Delta y \Delta z)$. (a) Pressures on the top and bottom y-faces that act over area $\Delta A = \Delta x \Delta z$ but differ due a pressure gradient. (b) Shear stresses, K_{ij}, where first index is the face where the stress acts (the face outward normal is in the i-direction) and second index is the direction of the resulting force (the force acts in the j-direction).

https://doi.org/10.1017/9781139028806.003 Published online by Cambridge University Press

the net force in the y-direction per unit volume is $-\Delta p/\Delta y$, which approaches $-\partial p/\partial y$ in the limit of an infinitesimally small volume. Applying a similar approach for the x-direction and the y-direction, the net pressure force $\left(\mathbf{F}_{\text{press}}\right)$ in the limit of an infinitesimally small volume is based on the pressure gradient.

A similar result can be obtained for the viscous stresses, except that there are three components of stress applied to each surface face, as shown in Figure 2.2b. The viscous stress tensor, K_{ij}, has two indices, where the first indicates face and the second indicates direction. In particular, the stress acts on the face whose outward normal is in the i-direction and the resulting force is directed in the j-direction. Notably, the viscous stress tensor is symmetric $\left(K_{ij} = K_{ji}\right)$, as will be shown later.

If the viscous stresses on a given face are approximately uniform, the top face (pointing in the y-direction) with area $\Delta x \Delta z$ would include shear stresses K_{yx} in the x-direction and K_{yz} in the z-direction, as well as a normal viscous stress K_{yy} in the y-direction. Similarly, the bottom face would include shear stresses K_{yx} in the negative x-direction K_{yz} and the negative z-direction as well as a normal viscous stress K_{yy} in the negative y-direction. Therefore (as with pressure gradients), a shear-stress gradient is needed to impart a net force on the fluid volume. Assuming a uniform gradient in the i-direction for each of the stresses and applying the limit of an infinitesimally small volume, the resulting viscous force per unit volume $(\mathbf{G})$ can be written in tensor or vector form as follows:

$$G_i \equiv \frac{F_{\text{visc,i}}}{\forall_f} = \frac{\partial K_{ij}}{\partial X_j} \qquad \textit{for } j = 1, 2, \textit{and } 3. \tag{2.11a}$$

$$\mathbf{G} \equiv \frac{\mathbf{F}_{\text{visc}}}{\forall_f}. \tag{2.11b}$$

It should be noted that the result of (2.11a) employs tensor symmetry.

Combining the preceding forces, the momentum generation rate can be written as follows:

$$\dot{\mathbf{q}}_{\text{mom}} = \frac{\mathbf{F}_{\text{body}} + \mathbf{F}_{\text{surf}}}{\forall_f} = \frac{\mathbf{F}_{\text{body}} + \mathbf{F}_{\text{press}} + \mathbf{F}_{\text{visc}}}{\forall_f} = \rho_f \mathbf{g} - \nabla p + \mathbf{G}. \tag{2.12}$$

Including this generation rate into (2.3) and (2.4) with $\mathbf{q} = \rho_f \mathbf{u}$, the resulting momentum transport PDEs in Eulerian and Lagrangian form are given (after some manipulation) as follows:

$$\frac{\partial(\rho_f \mathbf{u})}{\partial t} + \nabla \cdot (\rho_f \mathbf{u} \otimes \mathbf{u}) = \rho_f \mathbf{g} - \nabla p + \mathbf{G}. \tag{2.13a}$$

$$\rho_f \frac{\mathcal{D}\mathbf{u}}{\mathcal{D}t} = \rho_f \mathbf{g} - \nabla p + \mathbf{G}. \tag{2.13b}$$

These are the celebrated Navier–Stokes equations, and these two forms can be related using mass conservation (2.6a) by writing the outer product for (2.13a) as follows:

$$\nabla \cdot (\rho_f \mathbf{u} \otimes \mathbf{u}) = \rho_f (\mathbf{u} \cdot \nabla)\mathbf{u} = \mathbf{u} \nabla \cdot (\rho_f \mathbf{u}). \tag{2.14}$$

https://doi.org/10.1017/9781139028806.003 Published online by Cambridge University Press

Note that (2.13b) could also have been derived by applying Newton's second law along the fluid path of a fluid element, where the LHS is the product of mass and acceleration of a fluid parcel (per unit volume), while the RHS is the total force being applied to the fluid element (per unit volume). In both cases, the viscous stresses are related to the flow field, as discussed later.

The relationship between the fluid viscous stress and the fluid element changes is effectively similar to relating stress and strain for a solid. In particular, the strain on a fluid element can be related to the rates of shape deformation and volumetric change, which can be expressed in terms of the fluid element velocity gradients. For Cartesian coordinates, the resulting linear relationship between viscous stresses and these rates is given as follows (White, 2016):

$$K_{ij} = \mu_f\left(\frac{\partial u_i}{\partial X_j} + \frac{\partial u_j}{\partial X_i}\right) + \mu_{bulk,f}\delta_{ij}\frac{\partial u_k}{\partial X_k} \qquad \textit{for } k = 1, 2, \textit{and } 3. \tag{2.15a}$$

$$\delta_{ij} = \begin{cases} = 1 & \text{if } i = j \\ = 0 & \text{if } i \neq j \end{cases}. \tag{2.15b}$$

The first term on the RHS of (2.15a) is the stress based on the rate of deformation strain, whereas the second term is based on the rate of volumetric strain, which employs the Kronecker delta $\left(\delta_{ij}\right)$ of (2.15b). The proportionality between stress and strain is based on two viscosities: the shear viscosity $\left(\mu_f\right)$ for the deformation strain, and the bulk viscosity $\left(\mu_{bulk,f}\right)$ for the volumetric strain. The bulk viscosity $\left(\mu_{bulk,f}\right)$, is sometimes called the second viscosity coefficient and is typically modeled with Stokes' hypothesis as follows:

$$\mu_{bulk,f} = -2\mu_f/3. \tag{2.16}$$

This result is formally appropriate for monoatomic gases with moderate compressibility but has been found to be quite reasonable for a wide range of flows, and so will be employed for the rest of this text. However, it may not hold under extreme conditions such as within a shock wave where extreme compressibility occurs over a short distance (Gad-el-Hak, 1995).

If one considers fluids where the density can be considered constant along the fluid path, the velocity divergence will be zero (2.8) so that the last term in (2.15a) is also zero. Such a divergence-free flow (2.8) yields the following:

$$K_{ij} = \mu_f\left(\frac{\partial u_i}{\partial X_j} + \frac{\partial u_j}{\partial X_i}\right) \qquad \textit{for density constant along fluid path.} \tag{2.17}$$

This result shows that the viscous stress tensor is symmetric $\left(K_{ij} = K_{ji}\right)$, such as $K_{xy} = K_{yx}$.

For spherical coordinates, the corresponding spherical stress tensor components for divergence-free flow with azimuthal symmetry (Figure 1.23) can be expressed as follows:

$$K_{rr} = 2\mu_f\frac{\partial u_r}{\partial r}. \tag{2.18a}$$

https://doi.org/10.1017/9781139028806.003 Published online by Cambridge University Press

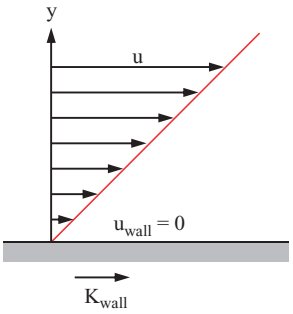

Figure 2.3 Shear stress acting on a stationary wall due to a velocity gradient caused by the no-slip condition, where direction of shear stress on the wall (K_{wall}) is in the direction of the flow. Due to an equal and opposite reaction, the stationary wall applies a shear stress on the fluid that is in the reverse direction.

$$K_{r\theta} = \mu_f \left[r \frac{\partial}{\partial r}\left(\frac{u_\theta}{r}\right) + \frac{1}{r}\frac{\partial u_r}{\partial \theta} \right]. \tag{2.18b}$$

$$K_{\theta\theta} = 2\mu_f \left[\frac{u_r}{r} + \frac{1}{r}\frac{\partial u_\theta}{\partial \theta} \right]. \tag{2.18c}$$

$$u_\phi = 0 \quad \textit{and} \quad \frac{\partial u_\theta}{\partial \phi} = \frac{\partial u_r}{\partial \phi} 0 \qquad \textit{for azimuthal symmetry}. \tag{2.18d}$$

Note that the spherical stress tensor is also symmetric (e.g., $K_{r\theta} = K_{\theta r}$).

If there is a solid surface, the viscous stresses will give rise to a shear force on the surface when there are velocity gradients. These gradients can arise since the fluid at the surface must accomodate the surface velocity (equivalent to 1.13). If we consider a stationary surface relative to our velocity reference frame (the surface velocity is zero), then this condition is given as follows:

$$\mathbf{u} = 0 \text{ at } \mathbf{X}_{surf} \quad \textit{no-slip condition at a stationary surface}. \tag{2.19}$$

If there is also a finite flow speed some distance away from the wall, this leads to a velocity gradient. For example, consider a flow in the x-direction, which has a linear velocity gradient in the y-direction, and is acting on a wall defined by $y = 0$, as shown in Figure 2.3. In this case, the wall shear stress K_{wall} equals K_{yx} since the face is normal to the y-direction and the shear force is in the x-direction. The no-slip condition in (2.19) yields $u_x = 0$ at $y = 0$, and the near-wall velocity gradient can be used to obtain the wall shear stress from (2.17) as follows:

$$K_{wall} = \mu_f (\partial u_x / \partial y)_{y=0}. \tag{2.20}$$

This stress acts along the wall surface and yields a force on the wall in the direction of the fluid (so the force of the wall on the fluid in the opposite direction).

https://doi.org/10.1017/9781139028806.003 Published online by Cambridge University Press

Returning to our governing equation, substituting either (2.17) or (2.18) into the momentum equation of (2.13a) and, assuming constant density and viscosity, yields the following:

$$\rho_f \frac{\partial \mathbf{u}}{\partial t} + \rho_f(\mathbf{u}\cdot\nabla)\mathbf{u} = \rho_f \mathbf{g} - \nabla p + \mu_f \nabla^2 \mathbf{u} \qquad \textit{for constant density and viscosity.} \tag{2.21}$$

This is the Eulerian momentum transport PDE for constant density and viscosity. The last term of the RHS includes the Laplacian of the fluid velocity, indicating that the viscous stresses effectively diffuse momentum. For example, consider the role of shear stress away from a wall, such as in a shear layer where there is a velocity gradient. In such flows, the higher-speed fluid imparts a shear stress in the direction of the flow and will transfer increased momentum to the lower-speed fluid. Similarly, the lower-speed fluid will impart a shear stress in the opposite direction on the higher-speed fluid and can serve to decrease its momentum. As such, viscous stresses tend to diffuse velocity gradients. Thus, one may consider viscosity as the effective diffusivity of fluid momentum caused by viscous stresses.

The assumption of constant viscosity used in (2.21) will generally be used in this text. However, it is worth noting that the viscosity can change with temperature. Interestingly, a temperature increase generally causes a decrease in liquid viscosity but causes an increase in gas viscosity. White (2016) provides viscosity–temperature relationships for several fluids. For dry air, the sensitivity for temperature in the range of 250–750 K can be approximated as follows:

$$\mu_f = \mu_{f,ref}(T/T_{ref})^{2/3}. \tag{2.22}$$

In this expression, $\mu_{f,ref}$ is the viscosity at $T_{ref} = 293$ K based on NTP conditions (per Table A.1). This relationship with a 2/3 exponent and a reference viscosity is also reasonable for several other gases in the range of 250–400 K (White, 2016).

Viscosity can also vary with fluid strain for some fluids, which are referred to as "non-Newtonian fluids." In particular, molten polymers and colloidal suspensions (e.g., paint) can have a nonlinear relationship between the velocity gradients and the viscous stresses, whereby the viscosity varies with the strain. However, this text will generally assume all fluids are "Newtonian" in that the viscosity does not depends on the strain on the fluid.

2.1.3 Transport of Energy and Species

Transport of Energy

For the fluid energy transport equation, we should consider both thermal and kinetic energy. The thermal (or internal) energy is related to the temperature of the fluid (stemming from vibration and random molecular motions of the fluid, which only come to rest when the temperature reaches 0 K). In contrast, the kinetic energy is related to the velocity of the fluid (stemming from mean molecular motion of the

https://doi.org/10.1017/9781139028806.003 Published online by Cambridge University Press

fluid). Combining these energies, the thermal energy per unit mass (e) plus the kinetic energy per unit mass ($\frac{1}{2}u^2$) yield the total fluid energy per unit mass (e_{tot}), as follows:

$$e_{tot} \equiv e + \frac{1}{2}u^2 \tag{2.23}$$

Setting the total fluid energy per unit volume ($q = \rho_f e_{tot}$) as the intensive scalar, the transport equation of energy can then be obtained by applying the Reynolds transport theorem. For energy, this is equivalent to using the first law of thermodynamics, whereby the energy change of a system per unit time is equal to the heat fluxing through the surfaces and the internal generation rate (the sum of internal energy release and work done on the fluid per unit time).

The fluid total energy transport equation can be obtained using (2.3) as follows:

$$\frac{\partial(\rho_f e_{tot})}{\partial t} + \nabla \cdot (\rho_f e_{tot}\mathbf{u}) + \nabla \cdot \mathbf{Q}_e = \rho_f \dot{e}_{tot}. \tag{2.24}$$

Special attention must be paid to the diffusive flux (last term on the LHS) and the internal generation (RHS).

The diffusive flux is nonzero because thermal energy can conduct due to molecular diffusion. This conduction can be obtained with Fourier's law, which states that the heat flux per unit area is equal to the product of the fluid thermal conductivity (k_f) and the gradient of fluid temperature, as follows:

$$\mathbf{Q}_e = -k_f \nabla T. \tag{2.25}$$

where the negative sign indicates that the energy moves from high temperature to low temperature.

The rate of internal generation of the total fluid energy inside a control volume can generally include the release of thermal energy by chemical reaction or phase change, as well as the increase of total energy by mechanical work on the fluid (e.g., a pump) or a decrease by fluid dynamic work done by the fluid within the control volume. Herein, we will generally neglect chemical reactions, radiation, phase changes, and mechanical work so that energy generation is only due to the fluid dynamic work done on the fluid. This work can be expressed as the dot product of the fluid dynamic forces and the fluid velocity. For example, the work rate per unit volume due to gravity forces is $\rho_f \mathbf{g} \cdot \mathbf{u}$. The pressure work rate on a fluid volume element can be considered as in Figure 2.2a. By considering pressure forces in all three directions, the pressure work rate per unit volume is $-\nabla \cdot (p\mathbf{u})$. Similarly, the viscous stress work per unit volume can be obtained as $\mathbf{G} \cdot \mathbf{u}$. Combining these elements with (2.24) and (2.25), the total fluid energy transport equation becomes

$$\underbrace{\frac{\partial(\rho_f e_{tot})}{\partial t}}_{\substack{\text{time rate of change} \\ \text{of total energy}}} + \underbrace{\nabla \cdot (\rho_f e_{tot}\mathbf{u})}_{\substack{\text{Convective flux} \\ \text{of total energy}}} = \underbrace{\rho_f \mathbf{g} \cdot \mathbf{u}}_{\substack{\text{Body force work}}} + \underbrace{\mathbf{G} \cdot \mathbf{u}}_{\substack{\text{Viscous} \\ \text{stress work}}} \underbrace{-\nabla \cdot (p\mathbf{u})}_{\substack{\text{Pressure} \\ \text{stress work}}} + \underbrace{\nabla \cdot (k_f \nabla T)}_{\substack{\text{Heat flux due to} \\ \text{thermal conductivity}}} . \tag{2.26}$$

https://doi.org/10.1017/9781139028806.003 Published online by Cambridge University Press

This PDE includes LHS terms of the time rate of change of total energy and the convective flux with RHS terms for the body force work, the fluid-stress work, and the heat flux due to thermal conductivity. As noted previously, this PDE neglects phase change (such as fluid evaporation or condensation), combustion or chemical reaction (which can lead to energy release), and radiation (which can lead to energy deposition or release) while also neglecting mechanical work and/or external heat transfer applied to the fluid.

In some cases, it is helpful to consider a transport PDE for the fluid temperature changes. In this case, the fluid internal energy per unit volume ($\rho_f e$) can be set as the transport quantity using (2.3) and the internal energy can be related to the fluid temperature and the specific heat at constant volume ($c_\forall$). If one further assumes an ideal gas with constant thermal conductivity, the internal energy and the temperature transport PDE can be expressed as follows:

$$e = c_\forall T. \tag{2.27a}$$

$$\frac{\partial(\rho_f c_\forall T)}{\partial t} + \nabla \cdot (\rho_f c_\forall T\, \mathbf{u}) = \mathbf{G} \cdot \mathbf{u} - \nabla \cdot (p\mathbf{u}) + k_f \nabla^2 T. \tag{2.27b}$$

The corresponding Lagrangian form for incompressible flow is then

$$\rho_f \frac{\mathcal{D}(c_\forall T)}{\mathcal{D}t} = \mathbf{G} \cdot \mathbf{u} - \nabla \cdot (p\mathbf{u}) + k_f \nabla^2 T. \tag{2.28}$$

The last RHS term in (2.27b) and in (2.28) includes a Laplacian of the temperature and is thus a diffusion term. As such, thermal conductivity acts to diffuse temperature gradients in a fluid (similar to how viscosity diffuses momentum gradients).

It is interesting to compare the rates at which thermal energy and momentum diffuse in a flow, where the effective diffusivity of momentum is proportional to viscosity (μ_f, with units of mass per distance per time), while the diffusivity of thermal energy is proportional to conductivity (k_f, with units of energy per distance per time per degrees Kelvin). To compare these diffusivities with the same units, the thermal conductivity can be divided by the fluid specific heat at constant pressure ($c_{p,f}$, with units of energy per mass per degrees Kelvin). The resulting nondimensional ratio of the momentum to thermal diffusivities is defined as the Prandtl number:

$$\mathrm{Pr}_f \equiv \frac{\text{viscous (momentum) diffusivity}}{\text{molecular thermal diffusivity}} \equiv \frac{\mu_f c_{p,f}}{k_f}. \tag{2.29}$$

As such, the Prandtl number of a fluid indicates how fast a velocity gradient is diffused compared to how fast a temperature gradient is diffused. Thus, a high Prandtl number indicates that velocity differences diffuse faster as compared to temperature differences. For steady conditions where diffusion and conduction are balanced, faster rates can be equated to achieving a fixed amount of diffusion over shorter distances. Thus, the Prandtl number will be proportional to the thickness of a thermal diffusion layer relative to a momentum diffusion layer.

For gases, the Prandtl number is on the order of unity (e.g., 0.7 for air at NTP), which indicates that rates of thermal and momentum diffusivity in a gas are similar.

https://doi.org/10.1017/9781139028806.003 Published online by Cambridge University Press

Thus, a thermal boundary layer (caused by the temperature difference between a freestream fluid and the surface) will have roughly the same thickness as that of a momentum boundary layer (caused by the velocity difference between a freestream fluid and the surface). However, the Prandtl number for liquids varies widely depending on the fluid type and temperature. For example, $\mathrm{Pr_f}$ ranges from 0.004–0.03 for liquid metals (very good heat conductors), ranges from 1.7–13.7 for water (a moderate conductor), and ranges from 50–100,000 for oils and polymer melts (poor heat conductors). For a fluid with a small Prandtl number (such as that seen in liquid metals), the thermal layers will be much thinner (or shorter lived) compared to the momentum layer so that thermal equilibrium can be expected to be achieved more quickly. The opposite would occur for fluids with a high Prandtl number.

Transport of Molecular Species

The final transport equation considered in this section is for molecular species. A species is a component of the fluid that has a singular molecule type. For example, nitrogen is a component species of air. The component fraction of a species in a fluid can be expressed in terms of the species mass fraction $(\mathcal{M})$ or the species density $(\rho_{\mathcal{M}})$, where the two are related by the overall fluid density (ρ_f) as follows:

$$\mathcal{M} \equiv \frac{\text{mass of a species}}{\text{mass of fluid mixture}}. \tag{2.30a}$$

$$\rho_{\mathcal{M}} \equiv \frac{\text{mass of species}}{\text{volume of fluid mixture}} = \rho_f \mathcal{M}. \tag{2.30b}$$

Since the species density equals the mass fraction of a species per unit volume, it can be summed over all species in the fluid to obtain the overall fluid density:

$$\rho_f \equiv \frac{\text{mass of fluid}}{\text{volume of fluid}} = \sum_{i=1}^{N_{species}} \rho_{\mathcal{M},i}. \tag{2.31}$$

In this expression, $N_{species}$ is the total number of species in a fluid (and i is a summation index).

Since the density of an individual species $(\rho_{\mathcal{M}})$ is an intensive quantity, its rate of change in a control volume is governed by the Reynolds transport theorem. If there are no chemical reactions (molecules do not change), the generation term for species will be zero, like that for mass. Species, such as mass and momentum, can be transported across the surface boundary by convection based on $\mathbf{u}$ (which represents the mean motion of molecules at a point). However, a species, can also be spread by diffusion through the random motion of molecules. For example, consider the spread of dye in water, where the dye represents an individual species (dye has a distinct chemical structure). If a drop of concentrated dye is released at one point in a container of still water $(\mathbf{u} = 0)$, the dye will slowly spread until its concentration is uniform and diluted throughout the container. Its spread is due to molecular diffusivity of one species (in this case, dye molecules) within a fluid (in this case, water molecules), where the mass diffusivity is denoted $\Theta_{\mathcal{M}}$.

https://doi.org/10.1017/9781139028806.003 Published online by Cambridge University Press

The molecular flux of a species in a miscible fluid can be described by Fick's law. This law states that the molecular flux per unit area for a species ($\mathbf{Q}_{\mathcal{M}}$) is the product of the molecular diffusivity ($\Theta_{\mathcal{M}}$) and the magnitude of the gradient of the species mass concentration ($\rho_{\mathcal{M}}$):

$$\mathbf{Q}_{\mathcal{M}} = -\Theta_{\mathcal{M}} \nabla \rho_{\mathcal{M}} = -\Theta_{\mathcal{M}} \nabla (\rho_f \mathcal{M}). \tag{2.32}$$

The negative sign on the RHS indicates that a species will flux in the direction from high-concentration to low-concentration regions. Note that $\Theta_{\mathcal{M}}$ is the diffusivity of species of mass fraction $\mathcal{M}$ relative to the overall fluid mixture, and thus is defined by both the species being considered and that of the surrounding fluid. For example, the diffusivity of oxygen in air is different from that in helium.

Applying the preceding diffusive flux to the RTT of (2.3) yields the Eulerian molecular species transport PDE, which is expressed as follows in terms of the species density and then in terms of the species mass fraction (both for the case where fluid density and molecular diffusivity are constant):

$$\frac{\partial \rho_{\mathcal{M}}}{\partial t} + \nabla \cdot (\rho_{\mathcal{M}} \mathbf{u}) = \nabla \cdot [\Theta_{\mathcal{M}} \nabla \rho_{\mathcal{M}}]. \tag{2.33a}$$

$$\frac{\partial \mathcal{M}}{\partial t} + \nabla \cdot (\mathcal{M} \mathbf{u}) = \Theta_{\mathcal{M}} \nabla^2 \mathcal{M} \qquad \textit{for constant } \rho_f \textit{ and } \Theta_{\mathcal{M}}. \tag{2.33b}$$

Note that the RHS of both equations includes no generation terms, since we have assumed no chemical reactions.

The PDEs of (2.33) state that the time rate of changes of species (the first term on LHS) stems from convective flux (the second term on LHS) and molecular diffusion (the RHS term). To understand the physics better, one may consider two limiting cases: (a) no time dependence and (b) no convection. For these two limits, (2.33b) becomes

$$\mathbf{u} = \Theta_{\mathcal{M}} \left(\frac{\nabla \mathcal{M}}{\mathcal{M}} \right) \qquad \textit{for steady local concentration field}. \tag{2.34a}$$

$$\frac{\partial \mathcal{M}}{\partial t} = \Theta_{\mathcal{M}} \nabla^2 \mathcal{M} \qquad \textit{for diffusion with no convection}. \tag{2.34b}$$

These two PDEs are considered in the following discussion.

For the steady condition with finite concentration gradients, the transport of species by convection in one direction must be balanced by diffusion in the other direction. Therefore, the effective diffusion speed is the RHS of (2.34a). This speed is based on the product of the species diffusivity ($\Theta_{\mathcal{M}}$, with units of length^2/time) and the normalized gradient (the term in in parentheses, with units of length^{-1}). Therefore, diffusion speed increases with the normalized concentration gradient, which scales inversely with the mixing layer thickness. For example, water vapor has a diffusivity of about 0.26 cm^2/s in air, so a gradient region of about 2 cm in thickness yields a local diffusion speed of about 0.13 cm/s.

For the zero-convection limit, (2.34b) indicates that the diffusion rate will be fastest when the Laplacian of the concentration is highest. For example, Figure 2.4a shows a

https://doi.org/10.1017/9781139028806.003 Published online by Cambridge University Press

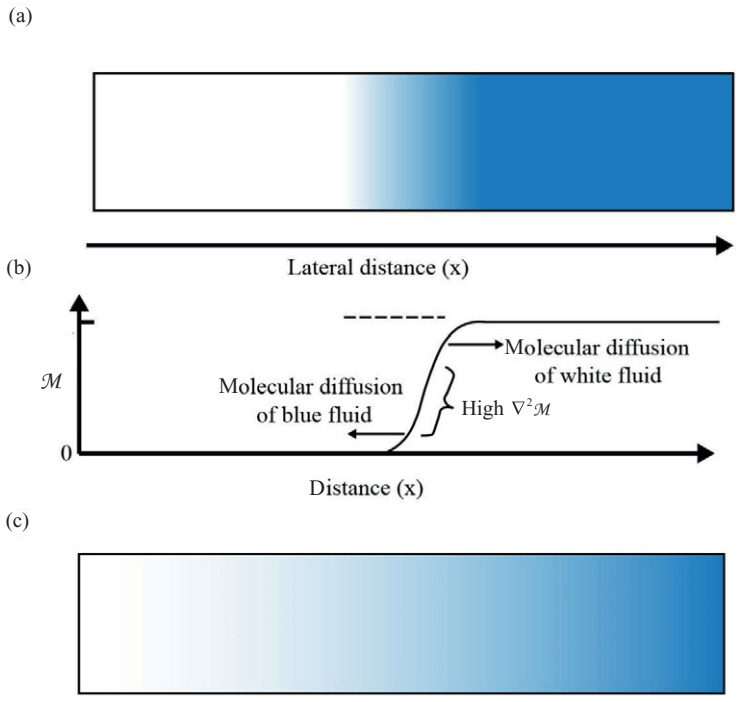

Figure 2.4 Mixing of fluids: (a) a white fluid on the left and a blue fluid on the right, showing an intermediate region where the two fluids are mixed; (b) instantaneous mass concentration of the blue fluid ($\mathcal{M}$), which will diffuse the fastest where the gradient is steepest and the diffusion direction will be the opposite direction of its gradient (blue fluid diffuses to the left); and (c) resulting mixing of both fluids at a later time due to molecular diffusion.

species (indicated by the blue color) that has a higher concentration in the right half of a container with still fluid. There will be a high gradient of this species at the mixing region (Figure 2.4b), causing the species to spread to the left, where the concentration is lower (consistent with negative RHS of 2.32). Over time, this spreading reduces the concentration gradients (Figure 2.4c), so the diffusion rate will lessen. Eventually, the species concentration will be uniformly distributed throughout the container. In this case, there are no more concentration gradients, so this uniform concentration will be the steady-state condition.

For most gas species, the species diffusivity is of the order of $10^{-5} - 10^{-4}\,\mathrm{m}^2/\mathrm{s}$. For most liquids, the species diffusivity is of the order 10^{-10} to $10^{-8}\,\mathrm{m}^2/\mathrm{s}$, which is many times smaller than that for a gas. Thus, the scent of a flower diffuses in a room of still air much faster than dye moves in a still pool. An increase in temperature will increase $\Theta_{\mathcal{M}}$ for both gases and liquids since temperature increases the random motion of molecules. Therefore, a fragrance diffuses faster in warm air. Molecular diffusivity is generally measured and empirically defined (like that for viscosity and thermal conductivity) at a reference temperature. For example, Table A.1 gives the NTP diffusivity of methane in air and of ethanol in water.

https://doi.org/10.1017/9781139028806.003 Published online by Cambridge University Press

To compare the spread rates of species to that for momentum, one may use the Schmidt number, which is defined as the momentum diffusivity normalized by the mass diffusivity:

$$\mathrm{Sc} \equiv \frac{\text{momentum diffusivity}}{\text{mass diffusivity}} \equiv \frac{\mu_f}{\rho_f \Theta_{\mathcal{M}}}. \tag{2.35}$$

For air and most gases, the Schmidt number is of order unity, indicating that the mass and momentum diffusion rates are similar. However, water and most liquids have small diffusivities (as noted earlier), which leads to high Schmidt numbers (e.g., on the order of 10^3). Mass diffusion is therefore much slower than momentum diffusion for a liquid. Thus, a small region of dye in still water will take much longer to spread out (to uniform concentration) compared to the time it takes for a small vortex in water to dissipate its velocity (to a still fluid).

2.2 Thermodynamic Closure and Flow Compressibility

In order to apply the previous conservation equations (for mass, momentum, energy, and species) when density and temperature vary, relations are needed to determine how these changes are related to changes in pressure and fluid energy. The relations are needed to ensure a closed set of equations for solution, and thus can be considered as the thermodynamic "closure" relations. These relationships are discussed in the following for both gases and liquids, followed by a discussion of flow compressibility's impact on velocity.

2.2.1 Thermodynamic Closures

The thermodynamic closure between pressure and density is often termed the *equation of state*. For gases, changes in pressure generally lead to significant changes in density. However, liquid density changes with pressure are often so weak that these changes are generally ignored. To determine when this is a reasonable assumption, one may consider a generalized equation of state that can apply to both liquid and gas compressibility via the empirical Tait equation:

$$\left(\frac{\rho}{\rho_{\mathrm{ref}}}\right)^{\mathcal{K}} = \frac{p + \mathcal{B}\, p_{\mathrm{ref}}}{(1+\mathcal{B})p_{\mathrm{ref}}} \quad \textit{Tait equation of state}. \tag{2.36}$$

This equation employs a compressibility exponent $(\mathcal{K})$, a pressure factor $(\mathcal{B})$, and reference values for density and pressure (ρ_{ref} and p_{ref}) at NTP conditions (Table A.1).

For liquids at isothermal (constant temperature) conditions, the constants $\mathcal{B}$ and $\mathcal{K}$ are much greater than unity; for example, values for water are $\mathcal{B}_\ell = 2,955$ and $\mathcal{K}_\ell = 7.15$ (Thompson, 1972, p. 289). These high values indicate that liquid density is a very weak function of pressure. For example, a 1% increase in water density at NTP conditions requires 200 atmospheres of pressure! Thus, water and most liquids

https://doi.org/10.1017/9781139028806.003 Published online by Cambridge University Press

are generally considered to be incompressible, so the density can be assumed to be constant.

For gases, there is no pressure factor $\left(\mathcal{B}_g = 0\right)$, and the pressure–density relationship via $\mathcal{K}$ depends on the thermal characteristics of the process. This relationship has two important thermodynamic limits: *isothermal* (constant temperature) and *isentropic* (constant entropy). These limits lead to different values of $\mathcal{K}$, as discussed in the following.

In an isothermal process, the ideal gas assumption (1.24) combined with constant temperature yields a simple linear relationship between pressure and density. The relationship can be expressed in terms of initial values for density and pressure (ρ_o and p_o) as follows:

$$\frac{\rho}{\rho_o} = \frac{p}{p_o} \qquad \textit{for gas in an isothermal process.} \tag{2.37}$$

Note that an isothermal process requires either work or external energy transfer to keep the temperature fixed if there is a volume change. For example, isothermal compression can be obtained if the process is very slow, so that high heat conduction to the surroundings ensures a constant internal temperature. Such an isothermal process requires an increase in fluid entropy.

For an isentropic process, it is important to first define the relationships with respect to temperature for changes in fluid internal energy (e) in terms of the specific heat at constant volume $(c_\forall)$ and for changes in fluid enthalpy $(h = e + p/\rho)$ in terms of the specific heat at constant pressure $\left(c_p\right)$:

$$c_\forall \equiv \left.\frac{\partial e}{\partial T}\right|_{\forall=\text{const.}} \tag{2.38a}$$

$$c_p \equiv \left.\frac{\partial h}{\partial T}\right|_{p=\text{const.}} = \left.\frac{\partial(e + p/\rho)}{\partial T}\right|_{p=\text{const.}} \tag{2.38b}$$

The ratio of these two specific heats (γ) is defined as follows:

$$\gamma \equiv \frac{c_p}{c_\forall}. \tag{2.39}$$

These relationships can be simplified by defining a "calorically perfect" gas as an ideal gas for which c_p and $c_\forall$, and thus γ are independent of temperature. The calorically perfect gas assumption allows a linear relationship between energy and temperature. For a gas, γ is related to the molecular degrees of freedom and for moderate temperatures equals 5/3 for a monatomic gas (like helium), and 7/2 for a diatomic gas (such as oxygen or nitrogen). The latter value $(\gamma = 1.4)$ is generally also used to describe the specific heat ratio for air at moderate temperatures.

To see how specific heats impact gas properties due to a temperature change, consider gas enclosed in a piston chamber, as shown in Figure 2.5. If the piston is locked in place (constant volume), an addition of heat will cause a gas temperature rise that is proportional to $c_\forall$, per (2.38a). If the experiment is instead conducted with a

https://doi.org/10.1017/9781139028806.003 Published online by Cambridge University Press

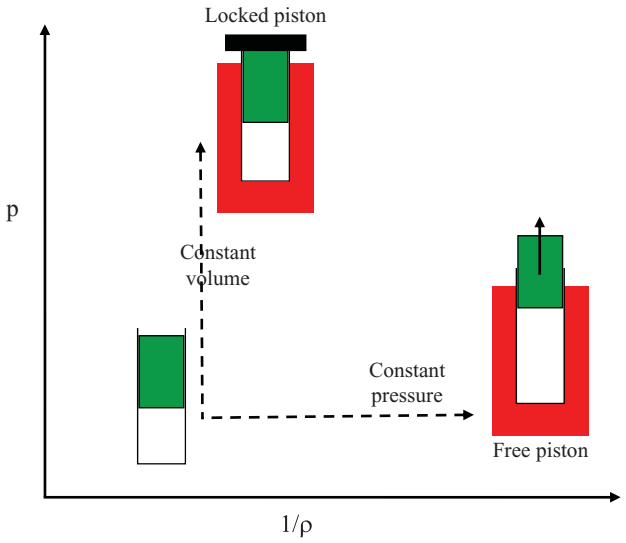

Figure 2.5 Pressure dependence on specific volume (inverse of density) for gas in a piston chamber based on two different heat-addition processes: a constant volume (locked piston) process and a constant pressure (free piston) process. The free piston requires γ-fold heat addition to have the same temperature rise as the locked piston.

free piston (where pressure is constant, so volume expands), an addition of heat causes a gas temperature rise that is proportional to c_p, per (2.38b). If both processes achieve the same temperature rise, the heat addition required for the free piston is γ times larger than that for the locked piston. Conversely, if both processes employ the same amount of heat addition, the temperature rise for the locked piston is γ times larger than that for the free piston.

If there is no energy transfer nor energy lost due to viscous dissipation, the process is reversible since the entropy is constant. This is referred to as an isentropic process. For a calorically perfect gas with isentropic conditions, the specific heat ratio can be used to relate the changes in pressure, density, and temperature (White, 2016), as follows:

$$\frac{p_g}{p_{o,g}} = \left(\frac{\rho_g}{\rho_{o,g}}\right)^{\gamma} = \left(\frac{T_g}{T_{o,g}}\right)^{\frac{\gamma}{\gamma-1}} \quad \textit{for gas in an isentropic process.} \tag{2.40}$$

To see the influence of heat transfer on pressure variations for a volume change, consider piston compression of a gas as shown in Figure 2.6. If the piston is insulated to ensure no heat transfer, the process is *adiabatic*. Thus compressing the chamber will cause an increase in density, temperature, and pressure. If this adiabatic process also has negligible energy losses due to gas viscosity, it will be an isentropic process and the pressure will rise with density per (2.40). If, on the other hand, the temperature is to be held fixed (isothermal), heat must flow outside of the control volume through the surface, such as by a cooling water jacket. In this case, the gas pressure rises linearly with density increase per (2.37).

https://doi.org/10.1017/9781139028806.003 Published online by Cambridge University Press

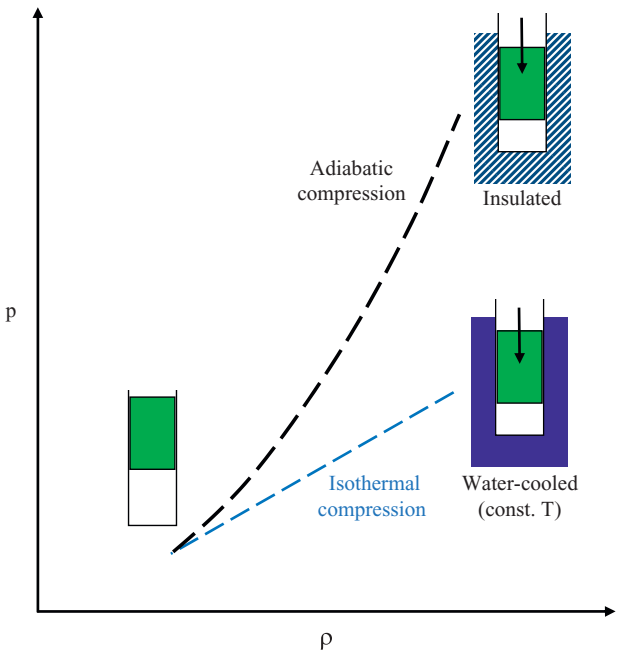

Figure 2.6 Pressure–density relationship for gas in a piston chamber for two compression processes with the same volume (density change) but different heat transfer conditions: adiabatic (no heat transfer through surface) and isothermal (no change in temperature).

One may also compare the pressure–density relationship for a gas compared to that for a liquid. If one converts (2.37) or (2.40) to the form of (2.36), the isothermal process for a gas is consistent with $\mathcal{K}_g = 0$ and $\mathcal{B}_g = 0$, while the isentropic process for a gas is consistent with $\mathcal{K}_g = \gamma$ and $\mathcal{B}_g = 0$. Thus, the Tait equation can be thought of as a generalized relationship that can apply to an isothermal gas, an isentropic gas, or a liquid for different limiting cases. The difference in the pressure–density relationship for an isentropic gas and for a liquid is qualitatively shown by the log–log plot of Figure 2.7. This shows that liquid densities are much higher than gas densities, but the log–log slope is also much higher ($\mathcal{K}_l = 7.15$ for water versus for $\mathcal{K}_g = 1.4$ air), since liquids are far less compressible.

Another important state relationship is between energy and velocity. For a calorically perfect gas, (2.38a) provides a linear relationship between temperature and fluid energy ($e = c_\forall T$) such that the total energy of (2.23) can be expressed as follows:

$$e_{tot} = c_\forall T + \frac{1}{2}u^2 \qquad \textit{for a calorically perfect gas.} \tag{2.41}$$

For a system with no heat transfer nor mechanical work applied to the fluid, the total energy (LHS) will be constant. In this case, the RHS is also constant so an increase in gas velocity will result in a decrease in temperature. These offsetting changes represent an increase in the mean motion of the molecules (related to velocity)

https://doi.org/10.1017/9781139028806.003 Published online by Cambridge University Press

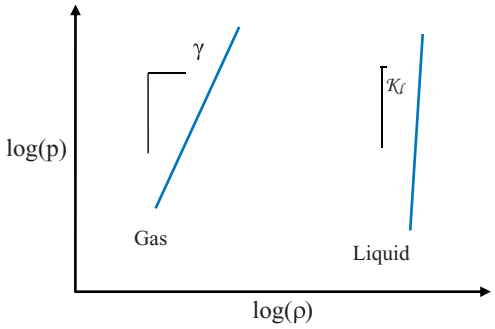

Figure 2.7 Pressure–density relationship for a liquid and an isentropic perfect gas (no work applied nor heat added).

at the expense of the random molecular motion (related to temperature). If the flow is also isentropic (frictionless), then this temperature decrease will be associated with pressure and density decreases based on (2.40).

2.2.2 Speed of Sound and Mach Number

The preceding relationships can also be used to define the acoustic speed of a fluid (a), also known as the speed of sound. This is the speed of pressure waves caused by a small isentropic density disturbance in an otherwise still fluid. As such, it can be expressed as follows:

$$a^2 \equiv \left.\frac{\partial p}{\partial \rho}\right|_{\text{const.entropy}} = \mathcal{K}\frac{(p + \mathcal{B}p_o)}{\rho}. \tag{2.42}$$

The RHS of (2.42) is obtained by assuming a calorically perfect fluid whose specific heats are constant. For a liquid, the speed of sound (a_l) is therefore given by the following:

$$a_l = \sqrt{\mathcal{K}_l(p + \mathcal{B}_l p_o)/\rho_l}. \tag{2.43}$$

For a gas in an isentropic process, the combination of (2.40) and (2.42) yields $\mathcal{B}_g = 0$ and $\mathcal{K}_g = \gamma$ so that the speed of sound is simply

$$a_g = \sqrt{\gamma \mathcal{R}_g T_g}. \tag{2.44}$$

The speed of sound for example fluids at NTP are given in Table A.1. The large $\mathcal{B}$ and $\mathcal{K}$ values for a liquid yield a high sound speed, such as 1,482 m/s for water. In comparison, the speed of sound for a gas is much lower, such as 343 m/s for air. The sound waves move in all directions at a speed relative to the local fluid velocity.

To determine the relative significance of acoustics and convection, the Mach number is defined as the ratio of flow velocity magnitude to the speed of sound:

$$M \equiv \frac{\text{convection speed}}{\text{acoustic speed}} \equiv \frac{u}{a}. \tag{2.45}$$

https://doi.org/10.1017/9781139028806.003 Published online by Cambridge University Press

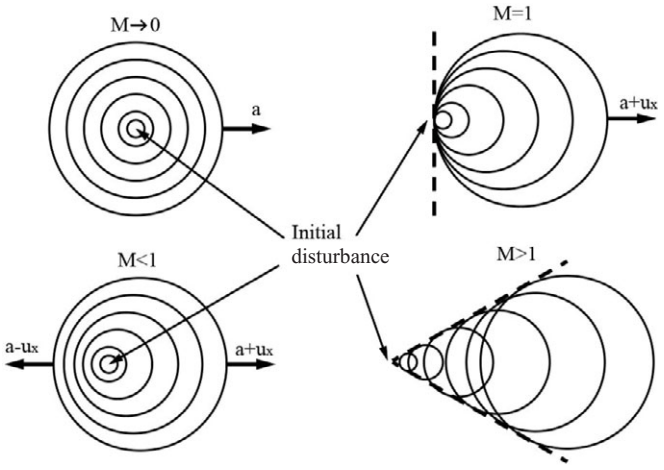

Figure 2.8 Acoustic waves as the Mach number changes from incompressible flow ($M \to 0$), subsonic flow ($M < 1$), sonic flow ($M = 1$), and supersonic flow ($M > 1$).

Since acoustic waves move at a speed relative to the flow convection, the Mach number gives rise to four different regimes as shown in Figure 2.8 and as listed in the following:

- $M \to 0$, incompressible flow, so waves travel at the same speed in all directions
- $M < 1$, subsonic flow, so waves travel faster in the downstream direction
- $M \sim 1$, transonic flow, so waves only travel in the downstream direction
- $M > 1$, supersonic flow, so waves travel only downstream in a Mach cone

As an analogy, consider a bridge over a river from which someone drops pebbles and looks at the waves relative to the bridge. If the river is moving very slowly, the waves travel in all directions. However, a faster river limits the upstream wave propagation speed seen from the bridge. In fact, no waves will travel upstream if the current if the river current is fast enough. The subsonic case can also be considered via acoustics, where the change in propagation speed gives rise to the Doppler effect for the sound of a train passing by a stationary listener. The sound frequency is higher as the train approaches, but then will be lower after it passes and is moving away.

To quantify how density varies with the Mach number, one may consider the one-dimensional versions of the momentum and energy PDEs (2.13 and 2.26) along a variable-area stream tube for isentropic flow. Based on (2.40) and (2.41), the pressure, density, and temperature all rise as the velocity slows down and these properties reach their maximum values when the flow stagnates. These values are referred to as the stagnation temperature, density, and pressure (T_{stag}, ρ_{stag}, and p_{stag}). The stagnation values may be combined with the Mach number definition to relate the more general values for a moving flow (Liepmann and Roshko, 1957) as follows:

https://doi.org/10.1017/9781139028806.003 Published online by Cambridge University Press

$$\frac{T_g}{T_{stag,g}} = \left(\frac{\rho_g}{\rho_{stag,g}}\right)^{\gamma-1} = \left(\frac{p_g}{p_{stag,g}}\right)^{\frac{\gamma-1}{\gamma}} = \left(1 + \frac{\gamma-1}{2}M^2\right)^{-1} \quad \textit{if isentropic}. \quad (2.46)$$

This relationship can also be used to determine when it is reasonable to assume the density is approximately constant with respect to velocity changes. For example, an isentropic acceleration from stagnation conditions to $M = 0.2$ yields a density reduction of 2% for $\gamma = 1.4$. As such, flows with $M < 0.2$ are widely considered to be incompressible. Note that $M < 0.2$ corresponds to flow speeds less than 68 m/s in air and less than 296 m/s in water. As such, many gas flows and the vast majority of liquid flows can be considered incompressible.

2.3 Incompressible Flow Characteristics

As discussed in §2.2, $M \to 0$ corresponds to incompressible flow, indicating changes in the flow velocity will not affect the fluid density along its path. If all other mechanisms that can cause changes in density (including combustion, heat transfer, and mechanical compression) are also negligible, then the density for a fluid element stays constant along its path, as follows:

$$\frac{\mathcal{D}\rho_f}{\mathcal{D}t} = 0 \quad \textit{for incompressible flow}. \quad (2.47)$$

However, constant density along a fluid path does not mean density is constant everywhere since a flow may be "stratified" with different densities. For example, atmospheric flows are generally stratified since higher altitudes tend to correspond to lower densities. Similarly, ocean flows can be stratified whereby regions of increased salt concentration are denser than those with less salinity. If stratification can also be neglected, the fluid density can be considered constant and uniform throughout, as follows:

$$\rho_f = \text{const.} \qquad \textit{uniform density flow}. \quad (2.48)$$

Such uniform density conditions significantly simplify flow analysis. In the following, we will consider three field characteristics for a constant density flow: stream function, vorticity, and velocity potential.

2.3.1 Stream Function

Flow streamlines about a body are an intuitive means of understanding a flow field. In two-dimensional flows, these streamlines can be quantified through the stream function (ψ) for incompressible flow. For such a flow, the velocity field has zero divergence (per 2.8), which be expressed in Cartesian or spherical coordinates (per 1.10a or 1.11a), as follows:

https://doi.org/10.1017/9781139028806.003 Published online by Cambridge University Press

$$\nabla \cdot \mathbf{u} = \frac{\partial u_x}{\partial x} + \frac{\partial u_y}{\partial y} + \frac{\partial u_z}{\partial z} = 0. \tag{2.49a}$$

$$\nabla \cdot \mathbf{u} = \frac{1}{r^2}\frac{\partial (r^2 u_r)}{\partial r} + \frac{1}{r \sin\theta}\left[\frac{\partial (u_\theta \sin\theta)}{\partial \theta} + \frac{\partial (u_\phi)}{\partial \phi}\right] = 0. \tag{2.49b}$$

If the flow is further limited to be two-dimensional in Cartesian coordinates ($u_z = 0$ and no gradient in the z-direction) or axisymmetric in spherical coordinates ($u_\phi = 0$ and no gradients in the ϕ-direction), the respective stream functions can be defined such that they satisfy the incompressibility condition:

$$\frac{\partial \psi}{\partial y} \equiv u_x \qquad \textit{and} \qquad \frac{\partial \psi}{\partial x} \equiv -u_y \qquad \textit{for } (x, y) \textit{ Cartesian flow}. \tag{2.50a}$$

$$\frac{\partial \psi}{\partial r} \equiv -r \sin\theta\, u_\theta \quad \textit{and} \quad \frac{\partial \psi}{\partial \theta} \equiv r^2 \sin\theta\, u_r \qquad \textit{for } (r, \theta) \textit{ spherical flow}. \tag{2.50b}$$

In particular, one may show that the stream function automatically satisfies incompressibility by substituting (2.50a) or (2.50b) into (2.49a) or (2.49b).

Once obtained, the stream function field can help describe the local flow characteristics. For example, lines of constant ψ help describe the instantaneous flow direction since these "streamlines" are everywhere parallel to the velocity. Furthermore, for steady flow, the volumetric flow between a pair of streamlines becomes constant. This means that the product of the velocity and the cross-sectional area is also constant, so a reduction in the gap between two streamlines indicates a local increase in velocity. Therefore, the flow streamlines give an indication of the velocity direction as well as the changes in velocity magnitude.

2.3.2 Vorticity and Irrotational Flow

While the stream function characterizes the direction of a fluid element relative to a fixed coordinate system, vorticity characterizes the rotationality of a fluid element about itself. In particular, vorticity ($\boldsymbol{\omega}$) is defined as the curl of the velocity field. In the following, we consider Cartesian and cylindrical forms of the vorticity. The vorticity vector for a Cartesian coordinate system and the associated vorticity magnitude are given as follows:

$$\boldsymbol{\omega} \equiv \nabla \times \mathbf{u} = \left(\frac{\partial u_z}{\partial y} - \frac{\partial u_y}{\partial z}\right)\mathbf{i}_x + \left(\frac{\partial u_x}{\partial z} - \frac{\partial u_z}{\partial x}\right)\mathbf{i}_y + \left(\frac{\partial u_y}{\partial x} - \frac{\partial u_x}{\partial y}\right)\mathbf{i}_z. \tag{2.51a}$$

$$\omega = \sqrt{\omega_x^2 + \omega_y^2 + \omega_z^2} \tag{2.51b}$$

The Cartesian vorticity components in (2.51b) are the three terms in parentheses in (2.51a), and the magnitude of the vorticity is a scalar field that shows the degree of rotationality throughout the flow.

The vorticity for a cylindrical coordinate system with the axial symmetry ($u_z = 0$ and no changes along the z-axis) is given as follows:

https://doi.org/10.1017/9781139028806.003 Published online by Cambridge University Press

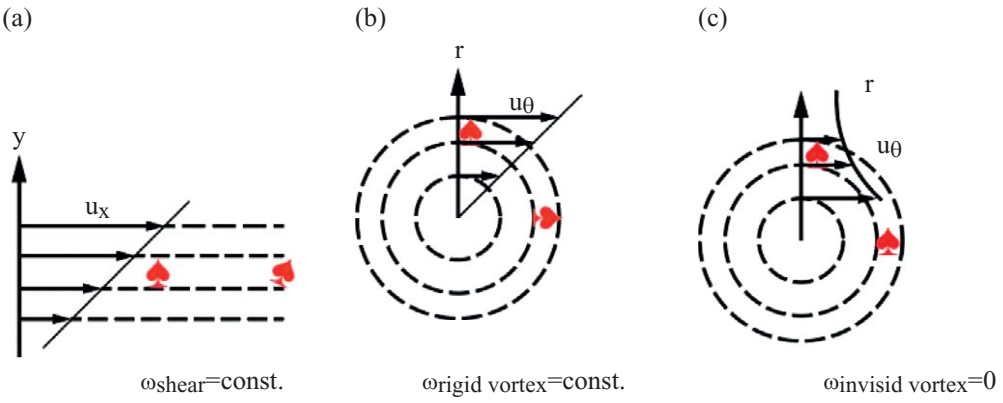

Figure 2.9 Schematic of simple flows, with dashed lines indicating streamlines and arrows indicating local velocity vectors for (a) linear shear flow, (b) rigid vortex, and (c) inviscid vortex. The flows include a marker (♠) that only rotates along a fluid path when there is vorticity, and thus does not rotate for the inviscid vortex.

$$\boldsymbol{\omega} \equiv \nabla \times \mathbf{u} = \frac{1}{r}\left(\frac{\partial(ru_\theta)}{\partial r} - \frac{\partial u_r}{\partial \theta}\right)\mathbf{i}_z \qquad \textit{for axial cylindrical symmetry.} \tag{2.52}$$

In this simplified flow, ω_z is the only vorticity component. A flow with finite (nonzero) vorticity for any of its components is considered a *rotational* flow.

Based on the two preceding forms in Cartesian and cylindrical coordinates, one may define two fundamental flows of uniform vorticity: the *linear shear* and the *rigid vortex* flows, which have only one velocity component. The linear shear flow has parallel streamlines (in one direction), but the velocity magnitude changes linearly in a direction normal to these streamlines. For example, Figure 2.9a shows a flow in the x-direction, where the speed (u_x) varies linearly with y. In this case, $\boldsymbol{\omega} = \omega_z \mathbf{i}_z$, and the vorticity magnitude describes the flow shear:

$$\omega_{shear} = \omega_z = \left|\frac{\partial u_x}{\partial y}\right| = \text{const.} \qquad \textit{linear shear flow.} \tag{2.53}$$

Such a shear flow can occur when a fluid moves along a wall where it must come to rest at the wall due to the no-slip condition (e.g., Figure 2.3) or when two fluids move in parallel but at different velocities (e.g., where a high-speed jet enters into a lower-speed surrounding flow).

The rigid vortex flow has cylindrical streamlines with a tangential velocity (u_θ) that increases linearly with radius (r), as shown in Figure 2.9b. In this case, the vorticity is given by the following:

$$\omega_{vortex} = \left|\frac{2u_\theta}{r}\right| = \text{const.} \qquad \textit{rigid vortex flow.} \tag{2.54}$$

This result shows that vorticity is equal to twice the fluid angular velocity. This is called a rigid vortex flow since it acts as if it is in solid body rotation (where viscosity is effectively infinite).

https://doi.org/10.1017/9781139028806.003 Published online by Cambridge University Press

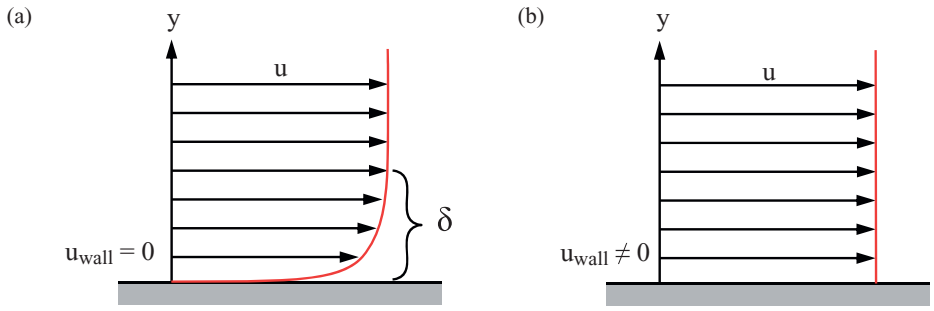

Figure 2.10 Simple velocity fields for flow past a stationary wall showing (a) no-slip conditions where viscosity effects cause the velocity to be zero at the wall ($u = 0$ at $y = 0$) resulting in a boundary layer thickness (δ); and (b) slip conditions where viscosity effects are ignored so that only the normal component of velocity is zero at the wall.

In contrast to the flows of (2.53) and (2.54), a flow with no vorticity is termed *irrotational*. An example of an irrotational cylindrical flow is the inviscid vortex given by the following:

$$u_\theta = \frac{\text{const.}}{r} \qquad \textit{inviscid vortex flow } (\omega = 0). \tag{2.55}$$

As shown in Figure 2.9c, the flow streamlines still circulate about the origin, but a fluid element in this flow does not rotate about itself (as shown by the marker in the figure). Therefore, this flow is irrotational.

In reality, most flows will have some portions that are rotational and other portions that are irrotational. For example, a circular vortex caused by a drain in a sink (or in the eye of a hurricane) will generally have a rotational inner core that follows (2.54) beyond which the vorticity will weaken and can eventually transition to an inviscid outer region that follows (2.55). Similarly, the two-dimensional flow over a wall can have a nearly linear shear near the wall per (2.53), but far from the wall the flow streamlines may be approximately dictated by irrotational flow. For example, the flow in Figure 2.10a shows a viscous rotational region of thickness δ beyond which $(y > \delta)$ the flow is approximately irrotational.

For a two-dimensional flow in the x-y plane, where ω_z is the only vorticity component, one may take the spatial derivatives of (2.50a) and substitute them into (2.51a). The result is a Poisson equation for the stream function and the vorticity given as follows:

$$\nabla^2 \psi = -\omega_z. \tag{2.56}$$

This result shows that the stream function can be used to determine the vorticity field (or vice versa) for a two-dimensional flow. However, a flow that is irrotational throughout allows additional characterization, as discussed in the following section.

2.3.3 Velocity Potential and Superposition

A flow that is irrotational $(\boldsymbol{\omega} = 0)$ gives rise to another flow field variable: the velocity potential, Φ. This field arises for zero vorticity since it corresponds to $\nabla \times \mathbf{u} = \mathbf{0}$ (per

https://doi.org/10.1017/9781139028806.003 Published online by Cambridge University Press

2.51), and since $\nabla \times (\nabla q) = \mathbf{0}$ for any scalar field q, the velocity potential can be set as q, as follows:

$$\nabla \Phi \equiv \mathbf{u}. \tag{2.57}$$

A flow for which Φ can be defined in this way is called a *potential flow*. While this requires the flow to be irrotational, it does not require the flow to be incompressible. However, if incompressibility is additionally assumed, this combination yields the following:

$$\left.\begin{aligned} \nabla \cdot \mathbf{u} &= \mathbf{0} \\ \nabla \times \mathbf{u} = \boldsymbol{\omega} &= \mathbf{0} \end{aligned}\right\} \quad \textit{for irrotational incompressible flow} \tag{2.58a, 2.58b}$$

If one combines (2.57) and (2.58a), it can be shown that the velocity potential satisfies a Laplacian PDE, and if one combines (2.56) and (2.58b) it can be similarly shown that the two-dimensional stream function also satisfies a Laplacian PDE:

$$\left.\begin{aligned} \nabla^2 \psi &= 0 \\ \nabla^2 \Phi &= 0 \end{aligned}\right\} \quad \textit{for irrotational incompressible flow} \tag{2.59a, 2.59b}$$

A key advantage of the Laplacian forms of (2.59) is that linear superposition can be used for stream functions and for velocity potentials. For example, the combination of three stream functions results in a new stream function that also satisfied (2.59):

$$\nabla^2(\psi_1 + \psi_2 + \psi_3) = \nabla^2\psi_1 + \nabla^2\psi_2 + \nabla^2\psi_3 = 0 = \nabla^2\psi. \tag{2.60}$$

A similar expression can be given for the combination of the velocity potentials and of the associated velocities. As a result, the combined stream function, velocity potential, and velocity field are the linear sums of the individual fields, as follows:

$$\left.\begin{aligned} \psi &= \psi_1 + \psi_2 + \psi_3 \\ \Phi &= \Phi_1 + \Phi_2 + \Phi_3 \\ \mathbf{u} &= \mathbf{u}_1 + \mathbf{u}_2 + \mathbf{u}_3 \end{aligned}\right\} \quad \textit{superposition of irrotational incompressible flows.} \tag{2.61a, 2.61b, 2.61c}$$

This superposition principle allows one to create a wide range of flow fields by combining fields of simple flows.

2.3.4 No-Slip versus Slip Boundary Conditions

As mentioned previously, flows often have rotational (viscous) and irrotational (inviscid) regions. For a stationary wall, viscosity results in a no-slip boundary condition, so the fluid velocity at the wall will be zero (per 1.13), which causes a velocity shear as shown in Figure 2.10a. However, inviscid flow allows a slip boundary condition on the surface so only the normal component will be zero (the tangential component is free), as shown in Figure 2.10b. These two boundary conditions can be expressed as follows:

https://doi.org/10.1017/9781139028806.003 Published online by Cambridge University Press

$$\mathbf{u} = 0 \qquad \textit{no-slip condition on a stationary wall.} \tag{2.62a}$$

$$\mathbf{u} \cdot \mathbf{n} = 0 \quad \textit{slip condition on a stationary wall.} \tag{2.62b}$$

Often, one may employ the slip boundary condition and the irrotational PDEs to help describe the flow far from the wall, whereas the no-slip boundary condition and the irrotational PDEs are needed to describe the flow near the wall and to describe the wall shear stress. These two limits of inviscid flow and viscous flow are considered in the next two sections.

2.4 Inviscid Incompressible Flow and Froude Number

2.4.1 Inviscid Irrotational Bernoulli Equations

If one can neglect the viscous effects, then the flow may be assumed to be irrotational. If one further assumes incompressible flow, then the conditions of (2.58) are satisfied. As shown in the following, the result allows us to directly relate pressure and velocity fields through the fluid momentum equation. To show this, the incompressible momentum transport of (2.21) for no viscosity can be expressed as follows:

$$\frac{\partial \mathbf{u}}{\partial t} + (\mathbf{u} \cdot \nabla)\mathbf{u} = -\frac{1}{\rho_f}\nabla p + \mathbf{g} \qquad \textit{for incompressible inviscid flow.} \tag{2.63}$$

One may use the vector dot product identity to rewrite the second term of this LHS as follows:

$$(\mathbf{u} \cdot \nabla)\mathbf{u} = \frac{1}{2}\nabla(\mathbf{u} \cdot \mathbf{u}) - \mathbf{u} \times (\nabla \times \mathbf{u}) = \frac{1}{2}\nabla u^2 - \mathbf{u} \times \boldsymbol{\omega}. \tag{2.64}$$

For zero vorticity, the second term on this RHS is zero and the remaining term can be substituted into (2.63). If the flow is also steady, (2.63) can be rearranged to express the pressure gradient as the sum of a dynamic component and a gravitational component:

$$\nabla p = -\tfrac{1}{2}\rho_f \nabla u^2 + \rho_f \mathbf{g} = (\nabla p)_{dyn} + (\nabla p)_{grav} \qquad \textit{if also steady.} \tag{2.65}$$

The first term on this RHS is the fluid dynamic pressure gradient (due to changes in velocity), and the second term is the gravitational pressure gradient (due to body forces). If gravity acts downward (in the negative y-direction), this second term can be expressed as follows:

$$(\nabla p)_{grav} \equiv \rho_f \mathbf{g} = -\rho_f g \mathbf{i}_y. \tag{2.66}$$

This term is sometimes called the *hydrostatic effect* because it determines the pressure increase with depth in still water.

Integration of (2.65) using the RHS of (2.66) can therefore be used to yield the "total" pressure field as follows:

$$p_{tot} \equiv p + \tfrac{1}{2}\rho_f u^2 + \rho_f g y = \text{const.} \qquad \textit{steady incompressible inviscid flow.} \tag{2.67}$$

https://doi.org/10.1017/9781139028806.003 Published online by Cambridge University Press

This is the irrotational Bernoulli equation and shows that the total pressure is constant throughout an incompressible irrotational steady flow field (not just along a streamline). This result also allows us to obtain the local flow pressure (p) given the local flow speed (u) and height (y).

For a fixed height, the stagnation pressure is the pressure recovered if the flow is brought to rest, and the corresponding pressure rise for this process is the dynamic pressure (p_{dyn}), as follows:

$$p_{stag} \equiv p + \tfrac{1}{2}\rho_f u^2 = \text{const.} \qquad (2.68a)$$

$$p_{dyn} \equiv \tfrac{1}{2}\rho_f u^2 \qquad \textit{for constant depth} \qquad (2.68b)$$

This relationship shows that the maximum pressure occurs when the flow comes to rest, while the minimum pressure occurs where the local flow speed is highest (note that $p_{stag} = p_{tot}$ at $y = 0$). A similar qualitative relationship between static and stagnation pressures was found for compressible flow as noted by (2.46).

2.4.2 Froude Number

The result of (2.67) can be simplified if the hydrostatic effects are negligible. To determine when this assumption is reasonable, one may compare effects of hydrodynamics to hydrostatics (on the RHS of 2.67) using a dimensionless parameter called the Froude number. To obtain this parameter, we identify the characteristic length in the gravitational direction as D_y and the characteristic speed as u_D, such as the body height and freestream velocity as shown in Figure 2.11a. We then assume that all other characteristic lengths

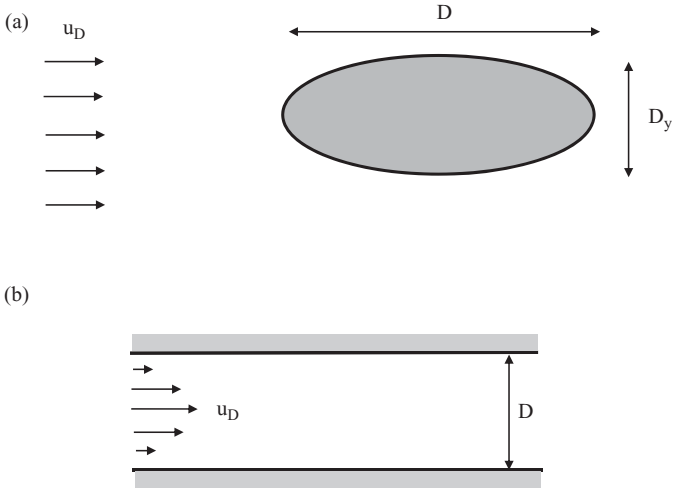

Figure 2.11 Example of characteristic flow scales for velocity and length, for (a) an external uniform flow over a body, which has a length D and a height D_y; and (b) an internal pipe flow that has a mean flow velocity based on u_D and pipe diameter D.

https://doi.org/10.1017/9781139028806.003 Published online by Cambridge University Press

and velocities in the domain are proportional to the characteristic length scale and velocity scale. These two values are then used to normalize the length and velocities in (2.65), while the pressure is normalized with twice the dynamic pressure (2.68b):

$$u^* = u/u_D. \tag{2.69a}$$

$$\nabla^* = D_y \nabla. \tag{2.69b}$$

$$p^* = p/\left(\rho_f u_D^2\right). \tag{2.69c}$$

Applying these nondimensional values to the steady-state version of (2.63) yields the following:

$$\nabla^* p^* = -\tfrac{1}{2}\nabla^* (u^*)^2 - \mathbf{i}_y / Fr_D. \tag{2.70}$$

The first term on the RHS represents the hydrodynamic effects, while second term represents the hydrostatic effects and is proportional to the inverse of the domain Froude number (Fr_D), which is given as follows:

$$Fr_D \equiv \frac{u_D^2}{gD_y}. \tag{2.71}$$

Thus, the Froude number represents the ratio of the convective effects (hydrodynamics) to the gravitational effects (hydrostatics).

The Froude number can be used to assess various flow limits. For $Fr_D \to 0$, the velocity effects are negligible so that hydrostatics determine the pressure gradient. For $Fr_D \to \infty$, the effect of hydrostatics is negligible so that the hydrodynamics determine the pressure gradient. Gas flows tend to have a combination of high velocities and smaller scales such that $Fr_D > 100$, so hydrostatic effects can be neglected. For liquid flows, the velocities are often smaller, so both effects can be important. For example, a submarine moving at 4 m/s with a body depth of 10 m yields $Fr_D = 0.25$, such that the hydrostatics will be roughly four times stronger than hydrodynamics. As another example, a fish at moving at 2 m/s with a body height of 10 cm has $Fr_D = 4$, so hydrodynamic effects will instead be roughly four times stronger.

2.5 Viscous Incompressible Flow and Reynolds Number

In this section, we retain our assumption of incompressible flow but reintroduce the effects of rotationality and viscosity in the momentum equation. The relative importance of these viscous effects is then quantified by the nondimensional Reynolds number.

2.5.1 Viscous Incompressible Flow Equations

For incompressible flow with constant viscosity, the continuity and momentum equations are respectively given by the Navier–Stokes equations of (2.8) and (2.21) and are restated as follows:

https://doi.org/10.1017/9781139028806.003 Published online by Cambridge University Press

$$\nabla \cdot \mathbf{u} = 0. \tag{2.72a}$$

$$\rho_f \frac{\partial \mathbf{u}}{\partial t} + \rho_f (\mathbf{u} \cdot \nabla)\mathbf{u} = \rho_f \mathbf{g} - \nabla p + \mu_f \nabla^2 \mathbf{u}. \tag{2.72b}$$

This is a closed set of PDEs since it contains two variables ($\mathbf{u}$ and p) and two equations. The equations can be expressed in Cartesian tensor form (with a repeated index indicating summation), as follows:

$$\frac{\partial u_i}{\partial X_i} = 0 \qquad for\ i = 1, 2, and\ 3. \tag{2.73a}$$

$$\frac{\partial u_i}{\partial t} + u_j \frac{\partial u_i}{\partial X_j} = g_i - \frac{1}{\rho_f} \frac{\partial p}{\partial X_i} + \frac{\mu_f}{\rho_f} \frac{\partial}{\partial X_j}\left(\frac{\partial u_i}{\partial X_j}\right) \qquad for\ j = 1, 2, and\ 3. \tag{2.73b}$$

The last term on the RHS of (2.73b) suggests the definition of kinematic viscosity:

$$\nu_f \equiv \mu_f / \rho_f. \tag{2.74}$$

The kinematic viscosity is effectively the momentum diffusivity per unit mass (instead of per unit volume as in μ_f) and has metric units of m^2/s.

For spherical coordinates with azimuthal symmetry (2.18d), the incompressible continuity equation, the momentum equations of (2.72) and the spherical Laplacian operator can be written as follows:

$$\frac{1}{r^2} \frac{\partial (r^2 u_r)}{\partial r} + \frac{1}{r \sin\theta} \frac{\partial (u_\theta \sin\theta)}{\partial \theta} = 0. \tag{2.75a}$$

$$\frac{\partial u_r}{\partial t} + u_r \frac{\partial u_r}{\partial r} + \frac{u_\theta}{r} \frac{\partial u_r}{\partial \theta} - \frac{u_\theta^2}{r} = g_r - \frac{1}{\rho_f} \frac{\partial p}{\partial r} + \nu_f \left[\nabla^2 u_r - \frac{2u_r}{r^2} - \frac{2}{r^2} \frac{\partial (u_\theta \sin\theta)}{\sin\theta\, \partial\theta}\right]. \tag{2.75b}$$

$$\frac{\partial u_\theta}{\partial t} + u_r \frac{\partial u_\theta}{\partial r} + \frac{u_\theta}{r} \frac{\partial u_\theta}{\partial \theta} + \frac{u_r u_\theta}{r} = g_\theta - \frac{1}{\rho_f r} \frac{\partial p}{\partial \theta} + \nu_f \left[\nabla^2 u_\theta + \frac{2}{r^2} \frac{\partial u_r}{\partial \theta} - \frac{u_\theta}{r^2 \sin^2\theta}\right]. \tag{2.75c}$$

$$\nabla^2 q = \frac{1}{r^2} \frac{\partial}{\partial r}\left(r^2 \frac{\partial q}{\partial r}\right) + \frac{1}{r^2 \sin\theta} \frac{\partial}{\partial \theta}\left(\sin\theta \frac{\partial q}{\partial \theta}\right). \tag{2.75d}$$

In the momentum equations of (2.75b) and (2.75c), the viscous terms are associated with the square brackets and kinematic viscosity.

2.5.2 Reynolds Number

To identify flow regimes with respect to the influence of viscosity, it is useful to simplify the conditions by neglecting gravitational effects (consistent with $Fr_D \to \infty$) and assuming steady flow. In this limit, the Cartesian momentum equation (2.73b) in vector and tensor form is as follows

https://doi.org/10.1017/9781139028806.003 Published online by Cambridge University Press

$$\rho_f(\mathbf{u}\cdot\nabla)\mathbf{u} = -\nabla p + \mu_f\nabla^2\mathbf{u}. \tag{2.76a}$$

$$u_j\frac{\partial u_i}{\partial X_j} = -\frac{1}{\rho_f}\frac{\partial p}{\partial X_i} + \nu_f\frac{\partial}{\partial X_j}\left(\frac{\partial u_i}{\partial X_j}\right) \qquad \textit{for } j = 1, 2, \textit{and } 3. \tag{2.76b}$$

The steady-flow assumption is reasonable if the boundary conditions and flow geometry are fixed in time (with no external forcing) and if the effects of viscosity are significant enough to prevent the flow from becoming unstable (as will be discussed later). The resulting PDE of (2.76) includes a convection term (LHS) as well as pressure and viscous terms (RHS). For most flows about a surface, pressure is critical to the surface stresses, regardless of whether the flow is viscous or inviscid. However, the convection and viscous terms are not always as critical. To characterize their relative influence, the momentum PDE can be made nondimensional but done such that pressure terms are always retained.

To make the PDE of (2.76) dimensionless, three characteristic scales are needed. For the first two, we employ a characteristic length scale (D) and a characteristic flow velocity (u_D), as shown in Figure 2.11. As an external flow example, D can be based on body length and u_D on the freestream velocity far upstream of the body. As an internal flow example, D can be based on a pipe diameter and u_D on the area-averaged flow speed through its cross section. The flow density (ρ_f) is used as the third scaling variable (as in 2.69c) in order to normalize pressure. The resulting dimensionless variables then become

$$\mathbf{u}^* = \mathbf{u}/u_D. \tag{2.77a}$$

$$\mathbf{x}^* = \mathbf{x}/D. \tag{2.77b}$$

$$p^* = p/\left(\rho_f u_D^2\right). \tag{2.77c}$$

Applying these dimensionless variables to (2.76a) yields the following:

$$\nabla p^* = -(\mathbf{u}^*\cdot\nabla)\mathbf{u}^* + \frac{1}{Re_D}\nabla^2\mathbf{u}^*. \tag{2.78}$$

The resulting momentum equation includes the domain Reynolds number (Re_D) defined qualitatively and quantitatively as follows:

$$Re_D \equiv \frac{\text{convection effects on pressure}}{\text{viscous effects on pressure}} \equiv \frac{\rho_f D u_D}{\mu_f}. \tag{2.79}$$

The quantitative definition of Re_D results from making the PDE dimensionless, while the qualitative definition stems from comparing the two terms on the RHS (the first is the convection term, and the second is the viscous term) of (2.78). The nondimensional PDE has two important consequences: similarity and characterization.

In terms of similarity, the solution to this dimensionless PDE will be the same for all flows of a given Re_D and domain shape. This flow similitude is often useful when conducting experiments. For example, the nondimensional velocity field obtained for a small model in a wind tunnel will be the same as that for a large model in flight so

https://doi.org/10.1017/9781139028806.003 Published online by Cambridge University Press

long as the $\mathrm{Re_D}$ and the geometry of the domain (boundaries and body) are the same. As such, the ratio of convection to viscous effects will only be a function of $\mathrm{Re_D}$ regardless of any changes in D, u_D, ρ or μ.

In terms of characterization, the PDE also shows that $\mathrm{Re_D}$ represents the relative importance of convection and viscous terms, which leads to various Reynolds number regimes, as discussed in the next section.

2.6 Reynolds Number Regimes

To characterize Reynolds number regimes, it is helpful to first define *laminar flow* as dynamically stable viscous flow. As such, a laminar flow has enough viscosity to prevent an unsteady perturbation from causing flow instabilities, so a flow will return to a steady state after it is perturbed. Therefore, laminar flows can only remain unsteady if they are continually driven by unsteady forces. For example, laminar blood flow is only unsteady due to the pulsatile nature of the heart. Since laminar flow is often steady, (2.78) is appropriate. The steady linear shear flow of Figure 2.10a is an example of a laminar flow (which is so named since these flows often have streamlines stacked in layers, i.e., in lamina).

In general, laminar flow is ensured when the viscous effects (relative to the convection effects) are large enough, which occurs when the Reynolds number is small enough $(\mathrm{Re_D} \ll 1)$. In particular, we define a critical Reynolds number $(\mathrm{Re_{D,crit}})$ as the maximum value for laminar flow with a given domain geometry, so the flow will be laminar if $\mathrm{Re_D} < \mathrm{Re_{D,crit}}$. In the following, we consider several Reynolds number regimes: $\mathrm{Re_D} \to 0$, $\mathrm{Re_D} \ll 1$, $\mathrm{Re_D} \sim 1$, and $1 \ll \mathrm{Re_D} < \mathrm{Re_{D,crit}}$ (all of which are laminar) as well as $\mathrm{Re_D} > \mathrm{Re_{D,crit}}$ (which includes transition to turbulence). For the laminar conditions discussed, we will assume there is no unsteady forcing nor effects of initial conditions, so the flow will be steady and (2.76) and (2.78) are generally applicable.

2.6.1 Laminar Flow Regimes

The limit of $\mathrm{Re_D} \to 0$ is called *creeping flow*, and such a flow is always laminar. If we apply this limit to the steady dimensionless momentum equation (2.78), the convection terms will be negligible compared to the viscous terms. Retaining the pressure term (since it is important for all Reynolds numbers), the resulting dimensional momentum PDE (assuming there is no unsteady forcing) becomes

$$\nabla p = \mu_f \nabla^2 \mathbf{u} \qquad \textit{for } \mathrm{Re_D} \to 0 \textit{ and steady flow.} \tag{2.80}$$

This result indicates that pressure stresses balance the shear stresses at every point in the flow. And because this PDE is linear, it is theoretically tractable for a variety of simple geometries and conditions.

https://doi.org/10.1017/9781139028806.003 Published online by Cambridge University Press

The next regime of $\mathrm{Re_D}$«1 occurs when the convection term in (2.78) has a finite but weak effect on the overall flow. In this case, the nonlinear convective term (LHS) can be linearized using the freestream velocity (u_∞) to obtain the following:

$$\rho_f(\mathbf{u}_\infty \cdot \nabla)\mathbf{u} = -\nabla p + \mu_f \nabla^2 \mathbf{u} \qquad \textit{for } \mathrm{Re_D} \ll 1 \textit{ and steady flow.} \tag{2.81}$$

This laminar flow regime is called *linearized flow* due to the convection term *linearization*. It has also been called *Oseen flow*, since this linearization was proposed by Oseen (1910) for the theory of flow over surfaces. Since (2.81) is a linear PDE, analytical solutions are available for simple geometries (e.g., parallel flow and small shape changes), and the results are often reasonable for $\mathrm{Re_D} < 0.1$. However, obtaining these solutions is often more complicated than for (2.80) due to the added convection term.

For the intermediate condition of $\mathrm{Re_D} \sim 1$, both the convective and viscous effects may have a strong influence on the pressure gradient. As such, convection cannot be generally neglected nor linearized, and instead must be retained in the steady momentum equation, as in (2.76), as follows:

$$\rho_f(\mathbf{u} \cdot \nabla)\mathbf{u} = -\nabla p + \mu_f \nabla^2 \mathbf{u} \qquad \textit{for } \mathrm{Re_D} \sim 1 \textit{ and steady flow.} \tag{2.82}$$

Some simple geometry cases still allow a theoretical flow solution for this laminar flow regime. In particular, a flow that is unidirectional with velocity gradients only normal to the flow will cause the LHS convection term to be zero, so the solution simply balances pressure stress and viscous stresses. For example, parallel flow between two plates (one fixed and one moving with the flow direction) gives rise to a linear shear flow, as in Figure 2.9a and the vorticity of (2.53). Other examples are the Poiseuille solutions for parallel flow in a circular pipe or between two plates (White, 2016). However, flows that change direction within the domain will cause the LHS convection term to be significant, which makes the PDE nonlinear and generally renders it analytically intractable unless the convection effects are weak.

If one considers the limit of $\mathrm{Re_D} \gg 1$, the convection effects may be much stronger than the viscous effects. If one further considers conditions where the flow is stable $(\mathrm{Re_D} < \mathrm{Re_{D,crit}})$ and is not subjected to unsteady forcing, the flow remains laminar and we retain the same PDE as (2.82):

$$\rho_f(\mathbf{u} \cdot \nabla)\mathbf{u} = -\nabla p + \mu_f \nabla^2 \mathbf{u} \qquad \textit{for } 1 \ll \mathrm{Re_D} < \mathrm{Re_{D,crit}} \textit{ and steady flow.} \tag{2.83}$$

For laminar flow at very high Reynolds numbers, one is tempted to assume that viscous effects are generally weak since they appear to be negligible when applying $\mathrm{Re_D} \to \infty$ for (2.78). However, viscous effects will be generally important for $\mathrm{Re_D}$»1 whenever there is a high shear region (e.g., due to the no-slip condition on a stationary surface). In fact, viscous effects will be strong for unidirectional flows with velocity gradients only normal to the flow (e.g., Poiseuille pipe flow) since the convection term will again be zero. Even when the flow is not unidirectional, viscous effects can still be important for $\mathrm{Re_D} \gg 1$ but are constrained to small regions where velocity shear is high but then can be negligible everywhere else.

https://doi.org/10.1017/9781139028806.003 Published online by Cambridge University Press

(a)

(b)

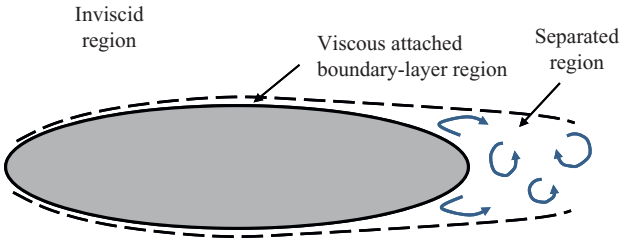

Figure 2.12 Flows with at $Re_D \gg 1$: (a) zoom-in of slowly growing boundary layer of local thickness δ along a flat plate of length D with uniform velocity above the plate; and (b) the boundary layer along an object of length D, where the flow separates of the aft surface (creating recirculating flow) whereby the viscous region is no longer thin and attached.

In particular, viscous effects will be significant very near any solid surfaces due to the no-slip condition, but an inviscid assumption may be reasonable for the rest of the flow. For example, the flow shown in Figure 2.12a has a velocity-gradient region (of height of δ) where viscous effects are important and determine the wall shear stress. This region is known as the *boundary layer* (Prandtl, 1904) and δ is the boundary-layer thickness. Above the boundary layer, the flow may be considered uniform and inviscid, as shown in Figure 2.12b. As may be expected, δ/D is small for a high Re_D (the thin boundary-layer assumption) but can vary greatly in size. For example, δ can be a kilometer for an atmospheric boundary layer or a few millimeters for the flow over a bird's wing.

As previously noted, a flow with $Re_D \gg 1$ with changes in flow direction can often be divided into small viscous regions and large inviscid regions. For flows over a body, the "inner region" is defined as near the surface with significant viscous effects, while the "outer region" is defined as an inviscid field away from the surface. The outer region can be described with the irrotational PDEs of §2.5. Employing the thin boundary-layer approximation ($\delta \ll D$), the inner region flow satisfies the two additional assumptions:

- The streamwise gradients are weak relative to the wall-normal gradients.
- The wall-normal velocities are small compared to the streamwise velocities.

Applying the preceding assumptions to the two-dimensional flow of Figure 2.12a, the steady x- and y-momentum equations are simplified (by neglecting small-order terms) as follows:

https://doi.org/10.1017/9781139028806.003 Published online by Cambridge University Press

$$\rho_f u_x \frac{\partial u_x}{\partial x} + \rho_f u_y \frac{\partial u_x}{\partial y} = -\frac{\partial p}{\partial x} + \mu_f \frac{\partial^2 u_x}{\partial y^2} \qquad \text{for a thin laminar boundary layer} \tag{2.84a}$$

$$\frac{\partial p}{\partial y} = 0 \tag{2.84b}$$

The first equation (2.84a) is the x-momentum whereby streamwise convection (LHS terms) is balanced with the streamwise pressure gradient and the tangential shear stress (RHS terms). The second equation (2.84b) is the y-momentum whereby the convection and stress terms are small compared to those in the first equation, so the wall-normal gradient is zero, yielding a constant pressure across the boundary layer thickness. Therefore, the inviscid pressure distribution just above the boundary layer is the same as the pressure distribution on the wall.

For the simplified case of a smooth flat plate in the x-direction with no streamwise pressure gradient, the theoretical velocity profile is given by the Blasius solution (White, 2016). This profile is a function of the wall-normal distance (y), the boundary-layer thickness (δ, defined as the height where the velocity is 99% of the freestream value), and the Reynolds number based on downstream distance (Re_x). The Blasius theoretical profile can be modeled as follows:

$$u/u_\infty \approx \tanh\left[1.65\, y/\delta + (y/\delta)^3\right] \tag{2.85a}$$

$$\delta \approx \left(5.29\, Re_x^{-1/2}\right) x \qquad \text{for laminar flow } (e.g., Re_x < 10^6) \tag{2.85b}$$

$$Re_x \equiv \rho_f u_\infty x/\mu_f \tag{2.85c}$$

This result shows that the velocity profile varies smoothly within the boundary layer and that the thickness increases with $x^{1/2}$.

For the more general case of a streamwise pressure gradient and/or wall curvature, the boundary layer may separate, as shown in part of Figure 2.12b. In this case, the thin boundary-layer approximation used in (2.84) is no longer applicable. Furthermore, such separated regions at high Reynolds numbers will generally become unsteady due to instabilities, leading to transitional or turbulent flow, as discussed in the following subsection (which will require a different PDE).

2.6.2 Transitional and Turbulent Flow Regimes

Flow fields are more likely to be inherently unstable as Re_D increases since the relative effect of viscous damping is reduced. This is particularly true if the flow is separated, which can occur at the rear section of a smooth body as shown in Figure 2.12b. This separation is more distinct at a sharp corner, as shown in Figure 2.13a. The boundary layer is attached upstream of the corner, but the flow separates just after the corner. This shear layer caused by this flow separation becomes unstable, yielding growing eddy structures (as discussed in §2.7). As such, this portion of the flow is no longer

https://doi.org/10.1017/9781139028806.003 Published online by Cambridge University Press

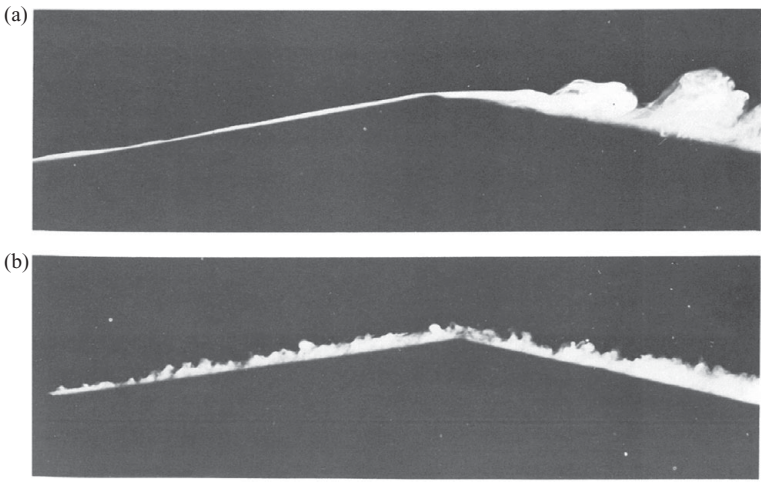

Figure 2.13 Boundary layers visualized with white dye at a high Reynolds number over a convex surface (Head, 1982): (a) laminar flow upstream that separates at the corner leading to an unsteady transition to turbulence; and (b) a turbulent flow upstream of the corner, which remains turbulent but attached after the turn.

laminar and instead includes a "transitional" region where the instabilities are growing though are primarily two-dimensional, followed by a "turbulent" region where the structures are three-dimensional and complex with a wide range of wavelengths.

If one considers the same corner geometry but with much higher Reynolds numbers, the transition to turbulence occurs for the portion upstream of the corner, as shown in Figure 2.13b. For a given geometry, the minimum Reynolds number for the transition to turbulence is designated as $\mathrm{Re}_{\mathrm{D,turb}}$. Comparing the boundary layers upstream of the corner as shown in Figures 2.13a and 2.13b, it can be seen that the turbulent one is thicker, which is due to the high degree of momentum mixing. This mixing makes a turbulent boundary layer fuller and more resistant to flow separation. This is evident in Figure 2.13b, where the boundary layer remains attached after the corner (whereas the laminar boundary layer of Figure 2.13a becomes separated).

Since transitional flows $(\mathrm{Re}_{\mathrm{D,crit}} < \mathrm{Re}_{\mathrm{D}} < \mathrm{Re}_{\mathrm{D,turb}})$ and turbulent flows $(\mathrm{Re}_{\mathrm{D}} > \mathrm{Re}_{\mathrm{D,turb}})$ are unstable, they are both governed by the three-dimensional unsteady Navier–Stokes equations:

$$\rho_{\mathrm{f}} \frac{\partial \mathbf{u}}{\partial \mathrm{t}} + \rho_{\mathrm{f}} (\mathbf{u} \cdot \nabla)\mathbf{u} = -\nabla \mathrm{p} + \mu_{\mathrm{f}} \nabla^2 \mathbf{u} \quad \textit{transitional or turbulent flow}. \tag{2.86}$$

These are the most difficult flow equations to solve (requiring computers) since they describe a complex flow field that is three-dimensional, unsteady, highly nonlinear, with a wide range of length and time scales, However, these equations are needed once the flow is turbulent or transitional.

The Reynolds number range for which transition occurs will vary with domain geometry. Generally, free boundaries, curvature, and corners tend to lower the critical

https://doi.org/10.1017/9781139028806.003 Published online by Cambridge University Press

Table 2.1 Reynolds number flow regimes and incompressible momentum equations in tensor notation (summation with j = 1,2,3).

Re	Regime	Momentum PDE
$Re_D \to 0$	Creeping flow	$\frac{\partial p}{\partial X_i} = \mu_f \frac{\partial}{\partial X_j}\frac{\partial u_i}{\partial X_j}$
$Re_D \ll 1$	Linearized flow	$\rho_f u_{j\infty}\frac{\partial u_i}{\partial X_j} = -\frac{\partial p}{\partial X_i} + \mu_f \frac{\partial}{\partial X_j}\frac{\partial u_i}{\partial X_j}$
$Re_D \sim 1$	Nonlinear flow	$\rho_f u_j\frac{\partial u_i}{\partial X_j} = -\frac{\partial p}{\partial X_i} + \mu_f \frac{\partial}{\partial X_j}\frac{\partial u_i}{\partial X_j}$
$Re_D \gg 1$, steady	Laminar boundary layer	$\rho_f u_x\frac{\partial u_x}{\partial x} + \rho_f u_y\frac{\partial u_x}{\partial y} = -\frac{\partial p}{\partial x} + \mu_f \frac{\partial^2 u_x}{\partial y^2}$
$Re_{D,crit} < Re_D < Re_{D,turb}$	Transitional flow	$\rho_f \frac{\partial u_i}{\partial t} + \rho_f u_j\frac{\partial u_i}{\partial X_j} = -\frac{\partial p}{\partial X_i} + \mu_f \frac{\partial}{\partial X_j}\frac{\partial u_i}{\partial X_j}$
$Re_D > Re_{D,turb}$	Turbulent flow	$\rho_f \frac{\partial u_i}{\partial t} + \rho_f u_j\frac{\partial u_i}{\partial X_j} = -\frac{\partial p}{\partial X_i} + \mu_f \frac{\partial}{\partial X_j}\frac{\partial u_i}{\partial X_j}$

Reynolds number for transition. In particular, the most unstable flows are those away from walls, such as separation regions, free-shear layers, wakes, and jets. For example, a planar shear layer can transition based on $Re_{\delta,crit} \approx 100$, where δ is the shear-layer thickness. A circular jet (with curvature) can have even greater sensitivity with $Re_{D,crit} \approx 50$, where D is the jet diameter. In contrast, flow in a pipe is stabilized by the presence of the walls. For example, a smooth circular pipe has $Re_{D,crit} \approx 2,300$. However, a pipe with a square cross section (whose corners promote instability) yields $Re_{D,crit} \approx 1,000$, and a curved pipe will also reduce $Re_{D,crit}$. An attached boundary layer along a flat plate (with a stabilizing surface and no curvature nor corners) can be stable up to $Re_{\delta,crit} \approx 3,500$, which corresponds to $Re_{D,crit} \approx 500,000$, where D is the plate length). Roughening the surface for flow in a pipe flow or on a wall will also make the flow less stable (introducing small corner and curvature flow around the roughness elements), reducing $Re_{D,crit}$. Therefore, flow geometry and Reynolds number both play key roles in the transition to turbulence.

2.6.3 Laminar vs. Transitional vs. Turbulent Flow

The various flow regimes and momentum PDEs discussed in the preceding section are summarized in Table 2.1. To see the differences between the flow regimes ranging from creeping flow all the way to turbulent flow, it is helpful to visualize the competing effects of diffusion to convection and the role of instability and unsteadiness.

To understand these effects, Osborne Reynolds in 1883 examined water flow in transparent pipes at various speeds and diameters by releasing a dye in the center of the pipe to visualize the onset of any flow instabilities. In these celebrated experiments, Reynolds found that a certain combination of diameter and flow speed yielded transition and turbulence (consistent with the Reynolds number criteria discussed

https://doi.org/10.1017/9781139028806.003 Published online by Cambridge University Press

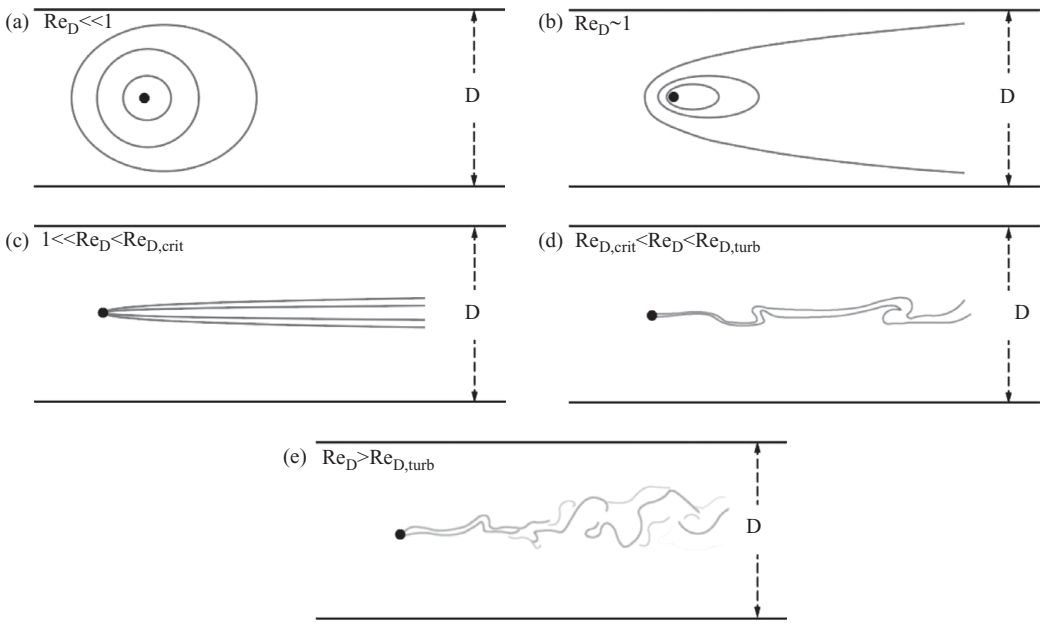

Figure 2.14 Illustration of the diffusion and convection of a fluid tracer species injected in a pipe center (at the black dot) for a left-to-right flow with (a) creeping flow, (b) flow with significant diffusion and convection, (c) high Reynolds number laminar flow, (d) transitional flow, and (e) turbulent flow.

previously). For a smooth circular pipe, the experiment of Reynolds and others are consistent with $Re_{D,crit} \approx 2,300$ and $Re_{D,turb} \approx 4,000$.

The dye experiment by Reynolds visualized the transition from laminar to turbulent flow. However, it cannot be used to readily investigate $Re_D (= \rho_f U_D D/\mu_f)$ effects within the laminar flow regime since the viscous diffusion rate will scale with μ_f/ρ_f while the dye diffusion rate will scale with $\Theta_{\mathcal{M}}$, and these two diffusivities are quite different for a liquid. In particular, the ratio of these two diffusivities is the Schmidt number $(Sc = \mu_f/\rho_f\Theta_{\mathcal{M}})$ and is of the order 10^3 for liquids. However, gases have a Schmidt number of order unity, so their momentum and mass diffusion rates are about the same. Therefore, visualizing the competing effects of convection to mass diffusion for a gas species will also approximately illustrate the competing effects of convection to viscous diffusion (which scale with Re_D). Based on this, we can construct a hypothetical experiment to investigate the Re_D regimes by considering the release of a tracer gas in a transparent pipe with an air flow and imagining that we can "see" the species concentration of the tracer gas within this airflow.

Using this approach, Figure 2.14 illustrates the flow conditions ranging from creeping flow to turbulent flow. For the creeping flow $(Re_D \ll 1)$ of Figure 2.14a, molecular diffusion (and thus viscous effects) dominate convection, so the tracer diffuses nearly radially outward from the point of injection. For $Re_D \sim 1$ of Figure 2.10b, downstream convection and upstream diffusion are of the same order

https://doi.org/10.1017/9781139028806.003 Published online by Cambridge University Press

(e.g., the balance indicated by 2.34a), so it much easier for the tracer to spread downstream. For the steady high Reynolds number laminar flow ($1 \ll Re_D < Re_{D,crit}$) of Figure 2.14c, convection will dominate diffusion, so the tracer moves primarily in the flow direction with only weak transverse diffusion. This is akin to a thin boundary layer where momentum diffusion is confined to a thin streamwise region.

If the Reynolds number is increased further such that $Re_D > Re_{D,crit}$ and the flow goes unstable as in Figure 2.14d, the flow is subjected to unsteady flow structures that serve to increase local mixing with lateral deviations (normal to the mean flow direction). At yet higher Reynolds numbers where the flow is turbulent ($Re_D > Re_{D,turb}$) as in Figure 2.14e, the flow contains complicated unsteady three-dimensional structures that substantially increase lateral mixing. This increased mixing causes the lateral distribution of the species to spread faster for turbulence than for laminar flow.

Since the turbulent regime leads to high mixing of momentum, this causes the profiles of the time-averaged velocity in the pipe to be much fuller than the velocity profile for laminar flow, as shown qualitatively by the profile insets in Figure 2.15. This is due to high-speed fluid in the pipe center region being moved toward the walls while low-speed fluid near the walls is transported toward the pipe center. Since the wall shear stress is proportional to the velocity gradient at the wall (recall 2.20), the fuller velocity profile for turbulent flow yields a larger average fluid shear stress on the

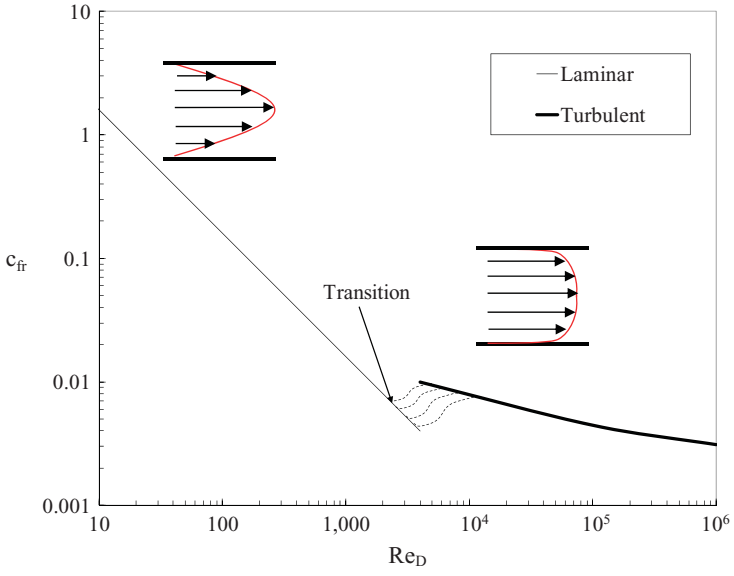

Figure 2.15 Fluid skin friction coefficient for a smooth fully developed pipe flow as a function of the pipe's Reynolds number for laminar flow ($Re_D < Re_{D,crit}$), transitional flow ($Re_{D,crit} < Re_D < Re_{D,turb}$), and turbulent flow ($Re_D > Re_{D,turb}$). The insets qualitatively indicate the shape of the time-averaged velocity profiles for laminar and mean turbulent flow.

https://doi.org/10.1017/9781139028806.003 Published online by Cambridge University Press

wall compared to that for laminar flow. These changes can be quantified using the fluid friction coefficient (C_{fr}) defined as the ratio of the time-averaged wall shear stress to the mean dynamic pressure, which can be related to the axial pressure gradient:

$$C_{fr} \equiv \frac{\overline{K}_{wall}}{\frac{1}{2}\rho_f u_D^2} = \frac{\partial \overline{p}}{\partial x}\left(\frac{D}{2\rho_f u_D^2}\right). \tag{2.87}$$

The LHS dimensionless parameter is also called the Fanning friction factor (and is one-fourth of the Darcy friction factor, which uses a different normalization).

Based on this definition, the friction coefficient for a circular straight pipe is plotted in Figure 2.15 for laminar, transitional, and turbulent flow. Laminar flow allows a theoretical Poiseuille flow solution (White, 2016), but a turbulent regime has no theoretical solution, so one must rely on empirical models based on experimental results, such as the Blasius empirical fit (White, 2016). These laminar and turbulent fluid friction values are both a function of the pipe Reynolds number:

$$C_{fr} = 16\,Re_D^{-1} \qquad \textit{for laminar pipe flow.} \tag{2.88a}$$

$$C_{fr} \approx 0.08\,Re_D^{-1/4} \qquad \textit{for turbulent pipe flow.} \tag{2.88b}$$

As shown in Figure 2.15, turbulence causes an increase in the skin friction coefficient, consistent with its fuller velocity profile. In between, there is a broad range of transition paths from laminar to turbulent flow. This is due to the high sensitivity of instability growth rate to small deviations in flow spatial or temporal uniformity. For example, slight changes in the entrance to the pipe or surface finish can cause significant changes in $Re_{D,crit}$ and $Re_{D,turb}$. Consequently, C_{fr} in the transitional regime is difficult to quantify, other than being bounded by the laminar and turbulent limits (2.88a and 2.88b).

For flat plates, the boundary layers have much fuller profiles when they are turbulent instead of laminar (like that for a pipe), as shown in Figure 2.16. The turbulent profile is "fuller" since most of the velocity distribution is close to the

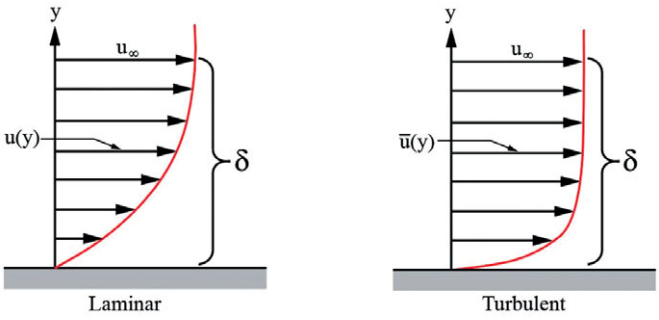

Figure 2.16 Velocity profiles for (a) laminar and (b) turbulent boundary layers of the same thickness, where the profile of the turbulent time-averaged velocity is much fuller near the wall, resulting in higher wall shear stress compared to that of the laminar boundary layer.

https://doi.org/10.1017/9781139028806.003 Published online by Cambridge University Press

freestream velocity. This fuller profile creates a higher-velocity gradient at the wall, thereby increasing fluid skin friction. For an airfoil, this leads to increased drag, which is generally detrimental to aerodynamic performance. However, the fuller velocity profile also increases the boundary layer's resilience to flow separation. In particular, turbulent boundary layers are more likely to stay attached on a convex surface compared to laminar boundary layers (Figure 2.13). For an airfoil, resilience to flow separation is generally favorable. As such, turbulence can lead to both positive and negative flow performance characteristics.

2.7 Flow Instability Mechanisms

The root cause for a flow to transform from laminar to transitional to turbulent conditions is flow instability. In particular, a flow can be considered unstable, stable, or neutrally stable. A flow is said to be unstable if an initial small perturbation grows larger over time as it convects. On the contrary, a flow is stable if the perturbations (with no further forcing) decays in amplitude over time. Energy dissipation by viscous stresses can cause such a decay. A neutrally stable flow will result in perturbations that neither grow nor decay.

In general, flow instabilities are related to the flow geometry and Reynolds number as well as the boundary conditions and any imposed forces. For example, flat plate boundary layers at high Reynolds numbers are subject to Tollmien–Schlichting instabilities stemming from streamwise disturbances that grow as they move downstream. These same types of instabilities can be found in pipe flow (Lessen et al., 1968) and other wall-bounded flows. Such wall-bounded instabilities require consideration of viscous effects and can be complex to analyze. However, two of the most common instabilities, Rayleigh–Taylor and Kelvin–Helmholtz, are inviscid and more readily analyzable. Their physics and frequencies are discussed in the following subsection.

2.7.1 Inviscid Flow Instabilities

One may investigate Rayleigh–Taylor and Kelvin–Helmholtz instabilities by considering two parallel-flowing incompressible immiscible inviscid fluids that have different densities and velocities, as shown in Figure 2.17. Since they are immiscible, the interface allows a density discontinuity where Fluid 1 (Figure 2.17a) has density ρ_1 and Fluid 2 (Figure 2.17b) has a density ρ_2. Since they are inviscid, the interface allows a velocity discontinuity where Fluid 1 has a velocity field $\mathbf{u}_1$ while Fluid 2 has a velocity field $\mathbf{u}_2$. The initial velocities for each fluid field are set as constants $(u_{1,o}, u_{2,o})$ with a flat interface at $y_I = 0$:

$$\left.\begin{aligned} u_1 &= u_{1,o} \quad \textit{with} \quad \rho_1 \quad \textit{for}\ y > 0 \\ u_2 &= u_{2,o} \quad \textit{with} \quad \rho_2 \quad \textit{for}\ y < 0 \end{aligned}\right\} \quad \textit{at}\ t = 0 \tag{2.89a, 2.89b}$$

https://doi.org/10.1017/9781139028806.003 Published online by Cambridge University Press

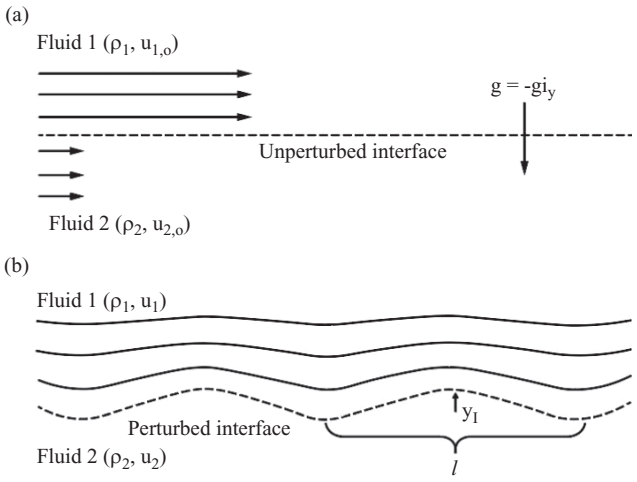

Figure 2.17 An irrotational incompressible flow with an interface that allows a velocity difference and/or a density difference: (a) initial conditions (no perturbations) with two fluids moving horizontally and with gravity vector as vertical; and (b) a later time with a perturbed interface (y_I) that has a wavelength (l) that impacts streamlines in the above fluid.

Since both fluids are incompressible and inviscid, their unsteady flow fields are each irrotational and so satisfy a Laplacian PDE for their velocity potentials (2.59b) as follows:

$$\nabla^2\Phi_1 = 0 \quad \textit{for flow in Stream 1.} \tag{2.90a}$$

$$\nabla^2\Phi_2 = 0 \quad \textit{for flow in Stream 2.} \tag{2.90b}$$

Notably, this irrotationality does not apply to the interface since it contains a discontinuous velocity difference, which is an infinitely thin vorticity layer. As such, the interface is hypothetical since viscosity would cause lead to a smoothly varying velocity change in a shear layer of finite thickness. Similarly, mass diffusivity would cause a smoothly varying density change.

Once the discontinuous interface is perturbed, it may become unstable depending on gravity and/or hydrodynamic effects. The perturbed interface (with height of y_I) can be modeled as a traveling sinusoidal wave that extends infinitely in the x-direction with perturbations in the y-direction (Figure 2.17b). This sine wave can be described in terms of an initial amplitude ($y_{I,o}$, which is a constant) as well as a wavelength (ℓ) and a frequency (f) as follows:

$$y_I = y_{I,o}e^{i(x/\ell - tf)}. \tag{2.91}$$

The wave thus moves in the x-direction at a speed of $f\ell$.

Since the interface joins the two fluids with no thickness, the velocities normal to the interface must be same on both sides (the tangential velocities can have a difference). If the curvatures are weak, the normal velocities can be approximated as

https://doi.org/10.1017/9781139028806.003 Published online by Cambridge University Press

the vertical velocities such that $u_{1y} = u_{2y}$ at the interface. This boundary condition can be expressed in terms of the velocity potentials (using 2.57) as follows:

$$\frac{\partial \Phi_1}{\partial y} = \frac{\partial \Phi_2}{\partial y} \quad \text{a } y = y_I. \tag{2.92}$$

If we neglect surface tension between the fluids, the pressure on either side of the interface will be equal. Based on this assumption, the pressure gradient in the unsteady Bernoulli equation (2.63) can be neglected at the interface, providing a second boundary condition:

$$\rho_1\left(\frac{\partial \Phi_1}{\partial t} + u_1\frac{\partial \Phi_1}{\partial x} + y_I g\right) = \rho_2\left(\frac{\partial \Phi_2}{\partial t} + u_2\frac{\partial \Phi_2}{\partial x} + y_I g\right) \quad \textit{at } y = y_I. \tag{2.93}$$

Note that the gravity force acts downward, so $\mathbf{g} = -g\mathbf{i}_y$, where g is a positive scalar. Far from the interface, the interface perturbations will have no effect, so

$$u_1 = u_{1,o} \quad \textit{for } y \to \infty. \tag{2.94a}$$

$$u_2 = u_{2,o} \ \textit{for } y \to -\infty. \tag{2.94b}$$

This provides the final flow boundary condition.

Since the flow is irrotational and incompressible, the linear superposition principle of (2.61b) can used to decompose the unsteady potential field as a sum of the initial unperturbed flow field (2.89 and Figure 2.17a) and the unsteady perturbations that travel with a wavelength and frequency (Figure 2.17b). Applying the boundary conditions of (2.92)–(2.94) for a given wavelength yields an ODE for the interface position (y_I) as a function of time and space (Drazin and Reid, 1981). Assuming weak perturbations, the two eigenvalues of the ODE are frequencies that can be expressed in terms of the fluid densities, far-field velocities, and the wavelength, as follows:

$$f = \frac{(\rho_1 u_{1,o} + \rho_2 u_{2,o}) \pm \sqrt{-\rho_1\rho_2(u_{1,o} - u_{2,o})^2 - (\rho_1 + \rho_2)(\rho_1 - \rho_2)g\ell}}{\ell(\rho_1 + \rho_2)}. \tag{2.95}$$

The interface perturbation will grow in time if this frequency has an imaginary component, that is, if the term within the square root is negative. This instability criterion is next considered for two special limiting conditions: (a) a density difference with initially uniform velocity; and (b) a velocity difference with initially uniform density.

The case of a density difference with no initial velocity $(u_{1,o} = u_{2,o} = 0)$ is a stratified flow for which (2.95) can be used to define the Rayleigh–Taylor instability frequency as follows:

$$f = \pm\sqrt{\frac{-(\rho_1 - \rho_2)g}{\ell(\rho_1 + \rho_2)}} \qquad \textit{for Rayleigh}-\textit{Taylor instability}. \tag{2.96}$$

If the above fluid is lighter than the below fluid $(\rho_1 < \rho_2)$, the term in the square root is positive, so the flow is theoretically stable to perturbations for incompressible and

https://doi.org/10.1017/9781139028806.003 Published online by Cambridge University Press

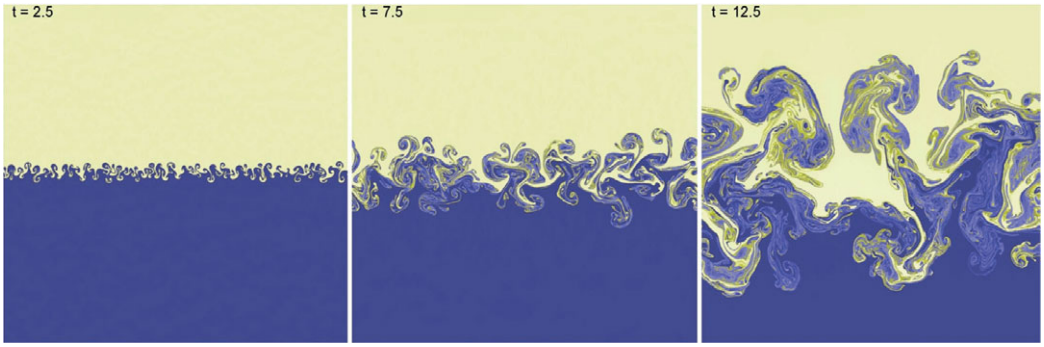

Figure 2.18 A heavier fluid over a lighter fluid that is perturbed and results in an evolving Rayleigh–Taylor instability (three different instances in times are shown), leading to larger and more complicated interface instabilities and flow structures at later times (Springel and Dullemond, 2011).

inviscid conditions. In particular, a perturbation to the interface will stably oscillate without growth (though any viscous damping would cause these oscillations to decay in amplitude). However, if the above fluid is denser than the below fluid $(\rho_1 > \rho_2)$, the flow is dynamically unstable, so any perturbations in the interface will grow exponentially with time. This is called the Rayleigh–Taylor instability. An example of this is shown in Figure 2.18, where a lighter fluid is placed below a heavier fluid. The smallest wavelengths grow quickest since these have the highest frequencies, per (2.96). However, larger and larger wavelengths occur over time, which cause the interface to become more convoluted, complicated, and distributed over a larger vertical extent. This generally leads to transition into turbulent flow if viscosity effects are small. And since this instability is due to the gravitational acceleration acting normal to the interface, a Rayleigh–Taylor instability can also grow whenever there is a fluid acceleration in the direction of the lighter fluid.

In the other limit of uniform density $(\rho_1 = \rho_2)$ with a velocity difference, a perturbation can lead to a Kelvin–Helmholtz instability. For the conditions shown in Figure 2.17a, the result of (2.95) for uniform density yields the following:

$$f = \frac{u_{1,o} + u_{2,o}}{2\ell} \pm \frac{\sqrt{-(u_{1,o} - u_{2,o})^2}}{2\ell} \quad \textit{for Kelvin}-\textit{Helmholtz instability}. \tag{2.97}$$

The first term on the RHS is the real part of the frequency and indicates that the convective speed of this perturbation $(f\ell)$ is equal to the average speeds of the two fluids, so $u_I = \frac{1}{2}(u_{1,o} + u_{2,o})$ The second term on the RHS is the imaginary part that of the frequency and indicates that any velocity difference across the shear layer (regardless of how small or which fluid is moving faster) will create instability.

While the Rayleigh–Taylor instability (heavy over a light fluid) is intuitive, the Kelvin–Helmholtz instability is more complex. To understand how this instability

https://doi.org/10.1017/9781139028806.003 Published online by Cambridge University Press

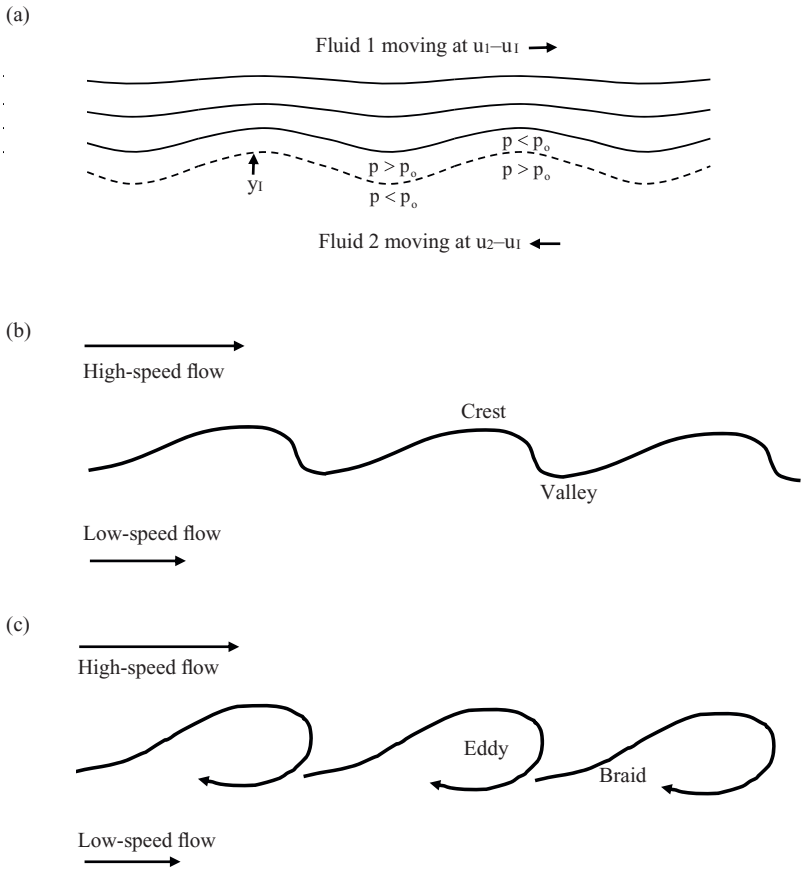

Figure 2.19 Kelvin–Helmholtz instability for two flows moving past each other with different speeds (and potentially different densities) separated by an inviscid interface: (a) a reference frame moving at speed of the sinusoidal interface (dashed line) creating variations in the high-speed fluid streamlines and the pressure field; (b) the local pressure decrease at a crest pulls it even farther upward while the local velocity increase pulls it faster to the right (and the opposite occurs for fluid in the valleys); and (c) a schematic of the eddy-and-braid flow after the amplified instabilities yield interacting vortex structures.

mechanism arises, we consider the local pressure relative to the initial pressure (p_o) in a reference frame moving with the interface speed (u_I). As shown in Fig. 2.19a for this reference frame, the high-speed fluid moves to the right and the low-speed fluid moves to the left. Since the flow is irrotational, the stagnation pressure within a given fluid is approximately constant (2.68a). As such, the local static pressure will be higher when the velocity is low ($p > p_o$ when $u < u_o$) and lower when the velocity is high ($p < p_o$ when $u > u_o$). Next we consider how the velocity varies due to the perturbation valleys and hills shown in Figure 2.19a. Since the flow is incompressible and since the high-speed flow is moving faster than the interface perturbation, continuity

https://doi.org/10.1017/9781139028806.003 Published online by Cambridge University Press

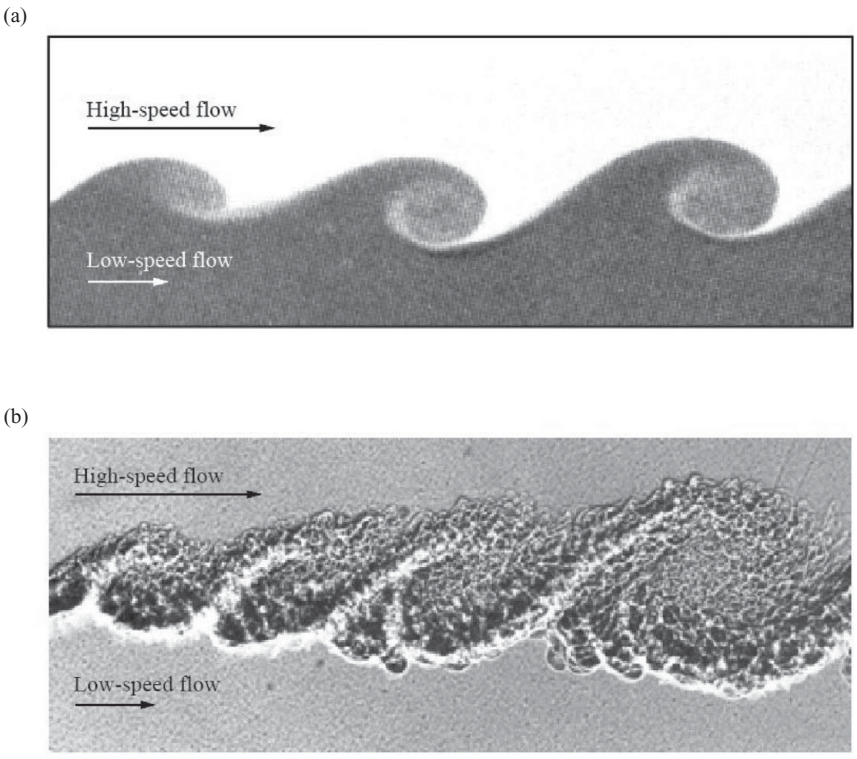

Figure 2.20 Images for parallel streams with different velocities where the shear-layer creates eddy-and-braid structures: (a) transitional conditions with moderate Reynolds numbers yielding two-dimensional flow (Thorpe, 1971); and (b) fully turbulent conditions at high Reynolds numbers yielding three-dimensional flow with a large range of length scales (Brown and Roshko, 1974).

(as discussed in §2.4) will cause Fluid 1 to decelerate in the valleys and accelerate at the crests. As such, the static pressure of the high-speed fluid will tend to be higher in the valleys and lower in the crests. If we consider the pressure field of Fluid 2, we find the opposite effect. Thus, the combination is a pressure difference in the direction of the surface perturbations. With no counteracting surface tension forces, this will cause the perturbations to grow. As such, this inviscid flow is always unstable. As a result, the Kelvin–Helmholtz instability is the most common instability mode in unbounded flows with velocity gradients (jets, wakes, free-shear flows).

Once the instabilities became large, the interface will no longer be represented by a simple sinusoidal perturbation. Instead, two-dimensional vortices will form whereby the fluid at the crest is moving faster on average and therefore pushes to the right and up, while the fluid in the valleys gets pushed to the left and downward (as in Figure 2.19b). As a result, the crest fluid eventually overtakes the valley fluid and the roll-up vortices lead to the "eddy-and-braid" features of Figure 2.19c.

https://doi.org/10.1017/9781139028806.003 Published online by Cambridge University Press

Note that the Kelvin–Helmholtz instability can be eliminated if there are competing forces that stabilize the interface or that dampen the perturbation energy. In particular, a stably stratified flow (lighter fluids moving above heavier fluids) can ensure the square root of (2.95) is positive for large enough wavelengths. Surface tension can add another stabilizing force that tends to be strongest at smaller wavelengths (higher curvatures). The addition of viscosity can diffuse the velocity gradients and dampen their energy, thereby reducing the growth rate of these instabilities. Therefore, the Kelvin–Helmholtz instability is more pronounced at higher Reynolds numbers (where viscous effects tend to be weaker), where it is more likely to induce turbulent flow.

For example, experimental results for parallel streams with velocity differences are shown in Figure 2.20, where the eddy-and-braid dynamics of Figure 2.19c can be observed. At the moderate Reynolds number for Figure 2.20a, the roll-up vortices are nearly two-dimensional, indicating transitional flow. For the higher Reynolds number of Figure 2.20b, the flow is fully turbulent, with a wide range of three-dimensional, unsteady, and effectively stochastic structures (as will be discussed in Chapter 6) superposed over the large-scale eddy-and-braid structures.

2.8 Chapter 2 Problems

As you work through the following problems, show all steps and list any needed assumptions.

(P2.1) A pond with a volume of 940 m^3 has an average fish birth rate of 2,500 per year and an average death rate of 3,800 per year. For two months a year, the pond is fed by a creek, which enters the pond with an average flow speed of 0.17 m/s, a cross-sectional area of 0.15 m^2 and a fish concentration of 0.02 fish/m^3. The pond has a spillover outlet to keep its volume constant, but a screen ensures no fish exit the pond. Starting from (2.1), apply the Reynolds transport theorem by drawing a control volume for the pond, define q and evaluate all terms to find the annual rate of change of the fish population for the pond.

(P2.2) Starting from the integral form of the Reynolds transport theorem (2.1), derive the Eulerian transport equation (2.3).

(P2.3) Consider a wind tunnel test with a 10 cm × 10 cm square cross section that is 1 m long, with steady air flow of 25 m/s. Upstream of the test section, there is a spray nozzle that injects droplets at the same speed as the air flow with an average drop diameter of 50 μm and a total mass flow rate of 10 grams per second. Within the test section, evaporation and wall impacts continuously remove 10% of the drop mass from the airstream. Apply the Reynolds transport theorem by drawing a control volume for the test section, defining an appropriate q variable for the transport of water drop mass in the test section, and quantitively evaluating all four terms (two are volume integrals and two are area integrals) in (2.1) based on this q.

https://doi.org/10.1017/9781139028806.003 Published online by Cambridge University Press

(P2.4) Starting with (2.3), (a) obtain the Eulerian x-momentum transport equation in component form (with u_x, u_y, u_z, K_{xx}, etc.) by setting the transport quantity $q = \rho u_x$, and by considering all the forces that act in the x-direction using a control volume diagram for pressure stresses and another for viscous stresses; and (b) then derive the PDE for $\mathcal{D}u_x/\mathcal{D}t$ assuming incompressible flow.

(P2.5) Consider a wind tunnel with incompressible inviscid steady flow moving in the positive x-direction (left to right) through a contraction with an air speed variation for $x > 0$ given as $u_o(1 + x/L)^{1/2}$, where $u_o = 0.25\ m/s$ and $L = 0.4\ m$. To analyze this flow, first decompose (2.21) into x- and y-momentum equations, where y is in the vertical direction. Then obtain the pressure gradients for air at normal density in the x- and y-directions at $x = 1\ m$.

(P2.6) (a) Starting from the control volume form of (2.1), derive the Eulerian species transport PDE using Fick's law for the diffusive flux, assuming constant molecular diffusivity. Then identify the physical interpretation of each term in the resulting transport equation. (b) Using the results from (a), and assuming incompressible flow, obtain the Lagrangian time derivative for the species mass fraction $(\mathcal{D}\mathcal{M}/\mathcal{D}t)$.

(P2.7) Consider steady quasi-one-dimensional air flow moving at 100 m/s and at NTP in a duct (Station 1) that then expands to twice the cross-sectional area at a downstream location (Station 2) with no change in altitude nor entropy. Employing (2.1) and (2.46), write two equations for M_1/M_2 and T_1/T_2 and use these together to solve for M_2, and then for pressure change $(p_2\text{-}p_1)$. (b) For an incompressible inviscid process for the same area change, find the resulting pressure change $(p_2\text{-}p_1)$. (c) Quantify and discuss the differences between the incompressible and isentropic pressure changes as related to the average flow Mach number. (d) For an isothermal process with the same velocity changes as in (a), is energy added to or extracted from the flow?

(P2.8) Consider a lake exposed to still dry air where the water vapor mass fraction in the air is 3% just above the water surface but reduces to 0% far away. At a height of 10 cm above the water surface, the vapor mass fraction gradient is 0.1%/cm and the diffusivity of the water vapor in air is $0.26\ cm^2/s$. Based on Fick's law, determine the mass flux per unit area of water vapor. Use this result to determine how much the lake level would change in one month.

(P2.9) Make a rough approximation of a horizontal slice of a hurricane as a solid body vortex for the interior (2.54 for $r < r_1$) and as an inviscid vortex for the exterior (2.55 for $r < r_1$), and assume both regions are incompressible with negligible radial and vertical velocities. At the interface $(r_1 = 100\ m)$, these two regions have the same pressure and tangential velocity $(u_1 = 40\ m/s)$ and the far-field $(r \to \infty)$ conditions are based on standard conditions for an altitude of 2,000 m (pressure of 79.5 kPa and a density of $1.01\ kg/m^3$). (a) Determine the radial distribution of the tangential velocity for both the

https://doi.org/10.1017/9781139028806.003 Published online by Cambridge University Press

exterior and interior regions. (b) Use these velocity distributions to determine the pressure at the interface (p_1) and at the vortex center (p_0).

(P2.10) Starting from (2.7b) and (2.13a), derive the mass and momentum PDEs of (2.72) in Cartesian coordinates, assuming a constant viscosity.

(P2.11) To define a nondimensional pressure, one may normalize by viscosity, $p^* = pD/(\mu_f u_D)$, instead of by density. (a) Starting from the PDE of (2.76b) and normalizing pressure by viscosity, derive a steady dimensionless form of the PDE in terms of Reynolds number. (b) Use this result to obtain the creeping-flow dimensional PDE for $Re_D \to 0$.

(P2.12) Consider a thin, two-dimensional, attached, laminar boundary layer along a wall in the x-direction with $Re_D \gg 1$. Starting from (2.83), obtain the relationships of (2.84).

(P2.13) Consider NTP flow of water in a pipe with an inner diameter of 4 cm. Determine the flow rate ranges (in liters per minute) corresponding to laminar, transitional, and turbulent flow regimes, then compute the axial pressure gradient at the start and at the end of the transitional flow range.

(P2.14) Consider a 5 m/s wind over initially stagnant water (e.g., a pond) at NTP. Determine which wavelength(s) can cause a small perturbation to grow into waves, assuming inviscid flow without surface tension. Discuss how surface tension and viscosity would affect these waves.

https://doi.org/10.1017/9781139028806.003 Published online by Cambridge University Press